APPENDIX A

Experimental Aspects: TGA

Page no

A.1. Calibration of rotameters

Calibration of the rotameters, was done with a Bunsen tower. The technique is based on the movement of a frictionless piston by the gas entering a vessel and measuring the time needed to displace a certain volume as indicated by the piston. The Bunsen tower employs a soap bubble moving upwards through a graduated burette. The soap bubble is the frictionless piston, implying that the pressure difference across the bubble is negligible, and the burette is used to measure the volume. The time it takes a bubble to travel along a certain length of the burette (corresponding to a certain volume) is determined with a stop-watch and the flow rate is thus determined. The size of the burette influences the linear velocity of the bubble and therefore affects the accuracy of time measurement and ultimately the flow rate measurement. Two Bunsen towers with different sizes were used to measure different flow rates. For large flow rates a larger burette ($400cm^3$) was used, while a small burette ($50cm^3$) was used for low flow rates.

A.2. Determining of the constant heat zone of the work tube

The temperature profile of the work tube was measured prior to the experimental runs. The profile is simply the variation of temperature with vertical position in the tube and indicates where the hottest area (with constant temperature) is located. Measurements were done by replacing the scale, molybdenum wire and crucible arrangement with a thermocouple. The thermocouple was lowered approximately 5 cm at a time, and held in position for at least ten minutes, while recording the temperature on a recorder. This procedure was repeated until the bottom of the work tube was reached. The temperature profile is shown in

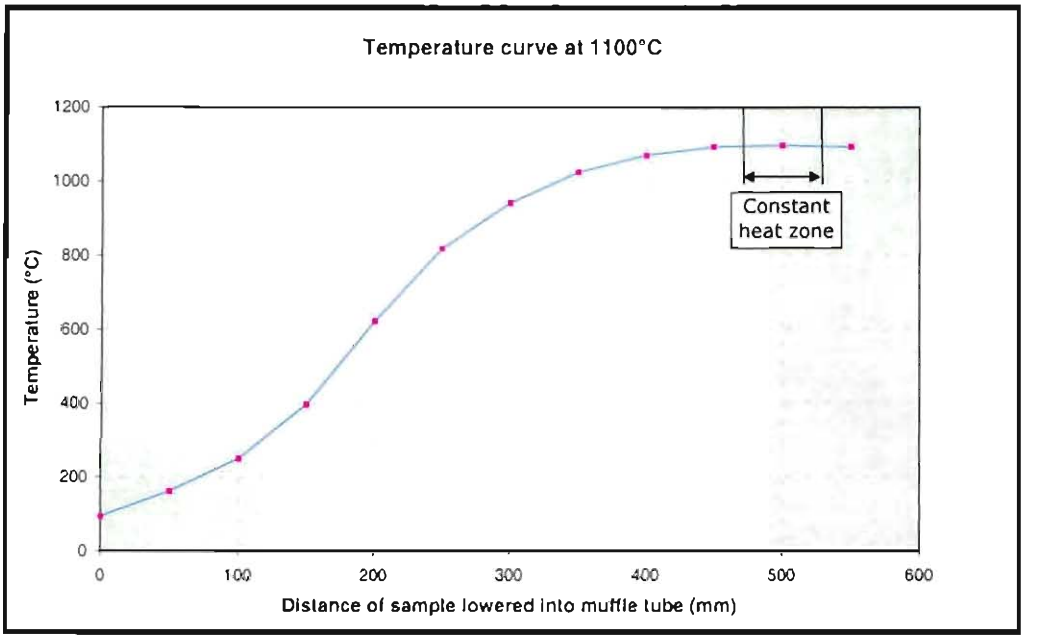

Figure A 1: *Temperature profile of the work tube that was used for thermo gravimetric analyses.*

A.3. Raw material preparation for TGA experiments

The feed materials for this investigation were similar to those used at the Ifcon pilot scale facility. The materials that were used are listed in ***Table A 1***.

Table A 1: *Feed materials used during this investigation.*

Feed Material	Ore
Ore	Iron ore fines (-10 mm) from Kumba's Sishen mine
	Iron ore fines (-10 mm) from Kumba's Thabazimbi mine
Coal	Duff coal from Eikeboom Collieries
	Duff coal from Leeuwpan Collieries
Dolomite	Fine dolomite from Mooiplaas dolomite mine
Limestone	Crushed sinter limestone from PPC Lime

All the materials were air dried for 24 hours. The coal was crushed, using a roller crusher. The gap of the crusher was set at 2 mm, and the material was fed slowly, to avoid choke feeding. Each batch of material was screened into distinct size fractions and each size fraction was weighed to obtain a size distribution for each batch of material. Note that only ore smaller than 6.3 mm, and coal, dolomite and limestone smaller than 2 mm were used. Oversize material was discarded. The screen analyses of the various feed materials are shown in ***Table A 2***.

Table A 2: *Size distributions that were used as standards for material make-up.*

	Mass percentage of material (%)			
Size fraction	**Ore**	**Coal**	**Dolomite**	**Limestone**
- 6300µm + 4750µm	31.12			
- 4750µm + 3350µm	20.62			
- 3350µm + 2800µm	7.50			
- 2800µm + 2000µm	12.07			
- 2000µm + 1400µm	7.75	43.49	13.77	49.73
- 1400µm + 850µm	6.74	23.65	32.08	12.62
- 850µm + 425µm	4.80	15.63	47.10	9.25
- 425µm + 212µm	2.05	17.23		5.88
- 212µm + 106µm	1.42		7.05	6.20
- 106µm	5.93			16.32
TOTAL (%)	**100.0**	**100.0**	**100.0**	**100.0**

These screen analyses were used as standard size distributions for all samples used during the experiments. This means that samples from each material stream was made up in such a way that the size distribution of a sample was similar to the distribution listed in ***Table A 2***. This ensured that the screen analyses of all the samples were similar. For example, the screen analyses of the Thabazimbi ore was modified to be similar to that of Sishen ore, and the screen analyses of the Leeuwpan coal was modified to be similar to that of Eikeboom coal.

Part of the coal was air dried for 24 hours, after which it was charred at 1000°C. The coal was charred until no further mass loss occurred. This was done by heating a 7 kg

batch of coal, at such a rate that 1% mass loss occurred every 10 minutes. Charring was done in a nitrogen atmosphere. After cooling, the char was screened and samples were compiled so that the size distribution of each sample matched the size distribution of the coal in ***Table A 2***.

A.4. Composition of raw materials

Two samples of each type of material were compiled for chemical analysis. The moisture content of the coal was determined by measuring the mass loss of the coal after air-drying the coal for 24 hours. The total carbon-, hydrogen-, oxygen- and nitrogen content of the coal was measured using a LECO analyser. The ash content of the coal and coal char was determined by combusting the coal (or char) with oxygen at 900°C.

Two ore samples, two dolomite samples and two limestone samples were pulverised, by milling each sample for 5 minutes in a pulverising mill. These samples as well as the ash were analysed using ICP (inductively coupled plasma) analyses. The chemical compositions of the ores and fluxes are shown in ***Table A 3*** while the moisture-, ash-, total carbon-, hydrogen-, oxygen- and nitrogen content of the coal and char are shown in ***Table A 4*** and ***Table A 5***. The chemical compositions of the ash from the coal and coal char are shown in ***Table A 6***.

Table A 3: *Average composition of ore and fluxes.*

Raw material	Units	Fe_2O_3	$CaCO_3$	$MgCO_3$	SiO_2	Al_2O_3	Total
Sishen ore fines	%	94.5	0.14	0.04	3.66	1.25	99.59
Thabazimbi ore fines	%	94.1	0.45	0.29	3.91	0.69	99.43
Dolomite	%	0.72	53.36	42.47	2.61	0.17	99.33
Limestone	%	0.21	95.49	2.18	1.13	0.17	99.17

Table A 4: *Ash and moisture content of coal and char.*

Raw material	Moisture (%)	Ash (%)
Eikeboom coal	1.6	12.5
Eikeboom char	0.3	15.7
Leeuwpan coal	1.3	14.8

Table A 5: *Total carbon-, hydrogen, oxygen, and nitrogen content of coal and char.*

Raw material	Units	C (%)	H (%)	O (%)	N (%)	Ash (%)	Total (%)
Eikeboom coal	%	72.9	3.97	8.36	1.88	12.5	99.6
Eikeboom char	%	82.1	0.33	0.37	1.10	15.7	99.6
Leeuwpan coal	%	71.6	3.58	7.58	1.80	14.8	99.3

Table A 6: *Ash composition of coal and char.*

Raw material	Units	Fe_2O_3	CaO	MgO	SiO_2	Al_2O_3	Total
Eikeboom coal	%	4.61	2.06	0.52	51.9	34.9	94.0
Eikeboom char	%	4.30	2.02	0.58	52.1	34.9	93.9
Leeuwpan coal	%	1.48	14.1	3.24	38.2	30.2	87.2

A.5. Analytical techniques

Ore-, lime-, dolomite-, ash-, and slag analyses were done by ICP (inductively coupled plasma) analysis. This method entails the melting of a known mass of the pulverised sample with sodium peroxide and carbonate as fluxes. The glass obtained from the melt is then dissolved in 20M hydrochloric acid. This solution is ionised in an argon plasma, and the intensity of the ionisation wavelengths are measured. Each element has one or more characteristic ionisation wavelengths and the measured intensities are recalculated to obtain the concentration of each element in the sample. The concentrations of the elements are expressed in terms of the most stable oxide (e.g. SiO_2) or simply as the concentration of the element in cases were the exact specie is not known (e.g. Fe which can be in the form of Fe_2O_3, Fe_3O_4, FeO_x or metallic Fe).

The forms of iron (i.e. Fe^0, Fe^{2+}, Fe^{3+}) were determined by wet chemical analyses. This method entails the dissolution of metallic iron (from a pulverised sample) with 10M iron

chloride ($FeCl_3$). The $FeCl_3$ oxidises all the metal iron (Fe^0) to Fe^{2+} ions in solution. The solution is then filtered. The Fe^{2+} content, of the filtrated solution, is determined by titration of the solution with potassium dichromate ($K_2Cr_2O_7$), which oxidises the Fe^{2+} to Fe^{3+}, while the Cr^{6+} from the chromate is reduced to Cr^{3+}. The titration yields the metallic iron content of the sample. The filtration residue, which contains all the Fe^{2+} (originally present as FeO), is dissolved in hydrochloric acid. The Fe^{2+} content of this solution is also determined by titration with potassium dichromate ($K_2Cr_2O_7$), which yields the Fe^{2+} content of the sample. Since the total iron content of the sample is known from ICP analysis, the Fe^{3+} content of the sample is calculated as the difference between the total iron content, the Fe^0 content, and the Fe^{2+} content.

The carbon and sulphur content of samples (excluding coal samples) were determined using a LECO CS 400 analyser, while the carbon, hydrogen and nitrogen content of the coal were determined with a LECO CHN 1000 analyser.

A.6. Raw material mixtures for TGA experiments

The mass ratio of coal to ore in the material mixture depends on the compositions of the coal as well as the composition of the ore. For this reason the atomic ratio of fixed carbon in the coal to reducible oxygen in the material mixture (further referred to as the $FC/O_{(red)}$ ratio) was calculated. The fixed carbon content of the coal was calculated from the total carbon-, oxygen- and hydrogen content of the coal. It was assumed that all the oxygen in the coal was present as moisture[15], while the hydrogen not associated with this moisture was reported as methane. This means that the fixed carbon was calculated as the difference between the total carbon content of the coal and the amount of carbon associated with the volatiles (as methane). The same argument holds for coal char.

The reducible oxygen is the oxygen associated with Fe in the material mixture. This was calculated from ICP analyses combined with the forms of Fe (discussed in ***Appendix A.5***).

The $FC/O_{(red)}$ ratio gives a good indication of the carbon efficiency of the process. In the Ifcon process, the carbon efficiency is determined by the CO/CO_2 ratio of the gas generated in the solids bed, the amount of carbon oxidised on the surface of the solids bed and the amount of carbon that reports to the molten bath[10,13,17]. The correct $FC/O_{(red)}$ ratio will result in just enough carbon at the bottom of the solids bed for complete reduction. When this ratio is too high, excess carbon is present at the bottom of the bed after reduction is completed. Most of this carbon will then dissolve into the

metal, thereby increasing the carbon content of the metal. When the $FC/O_{(red)}$ ratio is too low the material in the solids bed becomes depleted of carbon before reduction is completed. This will result in the production of a slag with high FeO content, which is associated with a low metal yield.

The material mixtures for the TGA tests were chosen so that the results of the experiments could be compared to results from the pilot scale facility and other relevant investigations[15,19].

A.7. Calculation of degree of reduction achieved

Since the mass of the sample was recorded continuously during the test, the degree of reduction achieved was calculated as a function of exposure time. Since exit-gas analyses were not available the quantitative contribution of carbon monoxide, hydrogen and hydrocarbons from volatiles, to the reduction reactions, was not known.

Two methods were used to calculate the degree of reduction achieved. The first method assumed that reducible oxygen was removed as a combination of CO, CO_2 and H_2O. The CO/CO_2 ratio was taken as that corresponding to the equilibrium CO/CO_2 ratio for the reduction of the oxide at 1000°C. 1000°C was an arbitrary estimate of the temperature at which the gas would leave the sample (noting that actual temperatures were not made). In addition, it was assumed that the volatiles acted as reductant, contributing to the reduction reaction. Results obtained by using this method of calculation are shown in ***Appendix C.2***

The second method assumed that oxygen (excluding oxygen present as moisture and CO_2 from calcination of $MgCO_3$) was removed only as carbon monoxide. The method was therefore based on the assumption that the outer surface of the sample heated up quickly to temperatures above 1000°C, and that the CO/CO_2 ratio was in equilibrium with the carbon on the outer surface of the sample. In addition, only the fixed carbon in the coal was considered as a reductant. The results obtained using this method are presented in ***Appendix C.3***.

The following generic assumptions were made for both methods described above:

a) Ca and Mg in the limestone and dolomite were present as $CaCO_3$ and $MgCO_3$ respectively.

b) The analyses were done on dry basis and the difference between the total of the ICP analyses and 100% represented elements not reported. The analyses were therefore normalized.
c) Oxygen in the volatiles was present as H_2O.
d) All hydrogen not accounted for as H_2O was present as CH_4.
e) The difference between the total carbon and carbon present as CH_4 resulted in the fixed carbon content of the coal.
f) Calcination of $MgCO_3$ were completed before reduction started.
g) Calcination of $CaCO_3$ only started once reduction was completed.

With both methods the degree of reduction achieved was calculated as a function of the exposure time.

APPENDIX B

Kinetic model inputs

B.1. Thermal conductivity correlations

The thermal conductivities of the iron oxide and carbon (with units W/m/K) was expressed as follows:

$$K=1/(AT+B) \qquad (B.a)$$

where *A* and *B* are constants shown in ***Table B 1***.

Table B 1: *Constants for calculation of thermal conductivities, with T_{max} signifying the maximum temperature over which the first set of values in the table (for A and B) are valid*[30]

Parameter	Iron oxide as O:Fe ratio			Carbon
	1.5	1.33	1.0	
A	1.84x10-04	1.69x10-04	2.34x10-04	0
B	0	0	0.1136	3.846
Tmax (K)	912	906	825	1600
A	8.32x10-05	2.97x10-06	0	0
B	9.24x10-02	0.1508	0.3062	3.846

Thermal conductivities for iron, the gas phase, lime and calcite(with units: W/m/K) was expressed as follows:

$$K=AT^2+BT+C \qquad (B.b)$$

where *A*,*B* and *C* were constants shown in ***Table B 2***.

Table B 2*: Constants for calculation of thermal conductivities*[30].

Constant	Fe	Gas phase	CaO	CaCO3
A	4.30x10-05	-2.46x10-08	0	0
B	-1.08x10-01	8.75x10-05	0	0
C	1.02x1002	2.05x10-03	1	1

B.2. Equilibrium constants

Expressions used to calculate equilibrium constants are presented in ***Table B 3***.

Table B 3: *Thermodynamic data used in model calculations*[30].

Reaction	Expression for equilibrium constant
$3Fe_2O_3 + CO = 2Fe_3O_4 + CO_2$ (above 564°C)	$pCO2/pCO = 10^{(3.8865-816.29/T)}$
$3Fe_2O_3 + H_2 = 2Fe_3O_4 + H_2O$ (above 564°C)	$pCO2/pCO = 10^{(2.2523-2034.4/T)}$
$Fe_3O_4 + CO = 3FeO + CO_2$ (above 564°C)	$pCO2/pCO = 10^{(0.6601-270.33/T)}$
$Fe_3O_4 + H_2 = 3FeO + H_2O$ (above 564°C)	$pH2O/pH2 = 10^{(2.2523-2034.4/T)}$
$FeO + CO = Fe + CO_2$ (above 564°C)	$pCO2/pCO = 10^{(-1.2239+ 1031.9/T)}$
$FeO + H_2 = Fe + H_2O$ (above 564°C)	$pH2O/pH2 = 10^{(0.4404 -806.56/T)}$
$0.25Fe_3O_4 + CO = 0.75Fe + CO_2$ (below 564°C)	$pCO2/pCO = 10^{(-0.3653+ 412.2/T)}$
$0.25Fe_3O_4 + H_2 = 0.75Fe + H_2O$ (below 564°C)	$pH2O/pH2 = 10^{(1.7157 -1706.95/T)}$
$CO_2 + C = 2CO$	$(pCO)2/pCO = 10^{(14.2423 -9016.9/T)}$
$H_2O + C = CO + H_2$	$pCO\ pH2O/\ pCO = 10^{(12.4224 -7009.2/T)}$

B.3. Enthalpy values

The enthalpy expression that was used was as follows:

$$H = A + BT \qquad (B.c)$$

Where H was the enthalpy (with units: J/mol), A and B were constants, and T was the absolute temperature (with unit: K). Values used for A and B are presented in ***Table B 4***.

***Table B 4**: Values used for the calculation of enthalpies*[30].

Species	A (J/mol)	B (J/mol K)
$FeO_{1.5}$	-435685	73.25
$FeO_{1.333}$	-393789	73.27
FeO	-283919	57.2
Fe	-19267	44.4
CO	-120780	32.33
CO_2	-411040	51.58
H_2	-9414	30.36
H_2O (g)	-254775	39.68
CH_4	-99500	65.58
C	-7924	20.42

B.4. Rate constants used in calculations

Rate constants and activation energies used for model calculations are presented in ***Table B 5***.

***Table B 5**: Rate constants and activation energies used for model calculations*[30].

Reaction	ko (m3/kg s)	EA (J/mol)
$3Fe_2O_3 + CO = 2Fe_3O_4 + CO_2$ (above 564°C)	30	69648
$3Fe_2O_3 + H_2 = 2Fe_3O_4 + H_2O$ (above 564°C)	133	54048
$Fe_3O_4 + CO = 3FeO + CO_2$ (above 564°C)	30	69648
$Fe_3O_4 + H_2 = 3FeO + H_2O$ (above 564°C)	133	54048
$FeO + CO = Fe + CO_2$ (above 564°C)	59	76887
$FeO + H_2 = Fe + H_2O$ (above 564°C)	214	65414
$0.25Fe_3O_4 + CO = 0.75Fe + CO_2$ (below 564°C)	0.20	26307
$0.25Fe_3O_4 + H_2 = 0.75Fe + H_2O$ (below 564°C)	1932	57053
$CO_2 + C = 2CO$	45780	172401
$H_2O + C = CO + H_2$	64	99814
	k (1/s)	EA (J/mol)
Devolatilisation (first step)	1.81x105	74000
Devolatilisation (second step)	8.99x108	157000

B.5. Default conditions for model calculations

Default conditions regarding used during model calculations are presented in ***Table B 6***.

***Table B 6**: Default conditions for model calculations*[30].

Parameter	Value
Furnace temperature	1473 K
Initial Fe content of the mixture	729 kg Fe/m^3
Initial fixed carbon content of the mixture	274 kg C/kg Fe
Volatile content (mass basis, ash free)	23%

APPENDIX C

TGA: Experimental results

C.1. Summary of experimental results

A summary of experimental data from the TGA tests that was used to calculate extent of reduction achieved as a function of time are presented in ***Table C 1*** to ***Table C 3*** below.

Tabel C 1: *Experimental results for base mixture*

Base mix 1 (1100°C)		Base mix 2 (1100°C)		Base mix 3 (1100C)		Base mix 4 (1100°C)	
Time	Mass	Time	Mass	Time	Mass	Time	Mass
(s)	(g)	(s)	(g)	(s)	(g)	(s)	(g)
0	86.62	0	88.08	0	85.98	0	89.36
103	84.75	104	86.28	103	84.40	104	88.08
207	82.40	208	83.98	207	82.13	208	85.72
311	80.53	312	82.04	310	80.28	311	83.83
415	78.98	416	80.45	413	78.72	415	82.21
518	77.77	521	79.19	516	77.46	519	80.86
622	76.73	625	78.13	620	76.38	624	79.74
725	75.85	729	77.23	725	75.47	728	78.77
828	75.11	833	76.48	828	74.72	832	77.92
932	74.45	937	75.83	932	74.07	936	77.22
1035	73.90	1041	75.30	1036	73.54	1040	76.61
1139	73.42	1144	74.83	1139	73.08	1143	76.06
1242	72.99	1248	74.42	1243	72.68	1247	75.61
1345	72.65	1352	74.10	1346	72.33	1351	75.21
1448	72.34	1455	73.83	3120	70.37	1454	74.85
1552	72.07	1559	73.61	3225	69.34	1558	74.55
1655	71.85	1662	73.41	3328	70.80	1661	74.30
1758	71.66	1766	73.26	3432	70.49	1764	74.08
1861	71.50	1869	73.13			1867	73.90
1965	71.36	1972	73.02			1971	73.74
2068	71.23	2075	72.92			2074	73.61
2171	71.13	2204	72.82			2177	73.51
2274	71.04	2307	72.75			2280	73.44
2377	70.96	2411	72.69			2384	73.38
2480	70.89	2513	72.64			2486	73.34
2584	70.83	2617	72.60			2589	73.30
2687	70.78	2720	72.56			2692	73.28
2790	70.73	2823	72.53			2796	73.25
2893	70.69	2926	72.50			2899	73.63
2996	70.65	3029	72.47			3002	73.64
						3105	73.64
						3208	73.64

Tabel C 2: *Experimental results for mixture containing Thabazimbi ore as well as the mixture containing Leeuwpan coal.*

Thabazimbi ore 1 (1100°C)		Leeuwpan coal 1 (1100°C)		Leeuwpan coal 2 (1200°C)	
Time	Mass	Time	Mass	Time	Mass
(s)	(g)	(s)	(g)	(s)	(g)
0	88.64	0		0	85.82
105	88.61	104	86.48	103	84.39
209	88.61	208	85.09	207	82.42
312	88.61	312	83.73	311	80.68
416	88.61	416	82.50	414	79.33
520	88.61	520	81.55	518	78.36
624	88.26	625	80.72	621	77.51
727	85.91	728	79.94	725	76.80
831	83.92	832	79.25	828	76.15
935	82.22	936	78.60	931	75.58
1039	80.80	1040	77.99	1035	75.05
1142	79.65	1143	77.42	1138	74.59
1246	78.70	1247	76.93	1242	74.19
1349	77.90	1350	76.49	1345	73.81
1453	77.22	1454	76.10	1449	73.51
1557	76.62	1557	75.74	1552	73.21
1660	76.12	1661	75.43	1655	72.93
1763	75.68	1764	75.15	1758	72.69
1866	75.30	1867	74.88	1862	72.50
1970	74.97	1970	74.64	1965	72.30
2073	74.67	2074	74.44	2068	72.15
2176	74.41	2177	74.25	2171	72.01
2279	74.20	2280	74.08	2274	71.89
2383	74.00	2384	73.94	2377	71.78
2486	73.83	2487	73.79	2480	71.68
2589	73.71	2590	73.67	2583	71.61
2692	73.59	2693	73.56	2686	71.51
2795	73.50	2796	73.47	2790	71.46
2898	73.40	2900	73.38	2893	71.41
3002	73.33	3002	73.31	2996	71.36
3105	73.27	3106	73.24	3099	71.32
3208	73.21	3209	73.18		
3311	73.16	3312	73.12		

Tabel C 3: *Experimental results for mixture containing Sishen ore with particle sizes as follows: +425 –850 µm, +1400 –2000 µm, +4750 –6300 µm..*

+212 -425 µm (1200°C)		+1400 –2000 µm (1200°C)		+4750 –6300 µm (1200°C)	
Time	Mass	Time	Mass	Time	Mass
(s)	(g)	(s)	(g)	(s)	(g)
0	86.07	0	89.22	0	85.82
104	84.44	104	87.53	104	84.39
208	82.26	208	85.30	207	82.42
312	80.48	312	83.40	310	80.68
415	79.05	416	81.90	413	79.33
519	77.90	520	80.67	516	78.36
623	76.95	624	79.59	619	77.51
727	76.06	728	78.71	722	76.80
831	75.33	831	77.90	825	76.15
934	74.69	935	77.22	928	75.58
1037	74.11	1039	76.63	1032	75.05
1140	73.63	1142	76.15	1135	74.59
1243	73.20	1246	75.73	1238	74.19
1346	72.82	1350	75.38	1341	73.81
1450	72.50	1453	75.06	1445	73.51
1553	72.22	1557	74.82	1548	73.21
1656	71.94	1660	74.60	1651	72.93
1760	71.71	1763	74.43	1754	72.69
1863	71.51	1867	74.30	1857	72.50
1967	71.33	1970	74.18	1960	72.30
2070	71.17	2074	74.08	2064	72.15
2173	71.03	2177	74.00	2167	72.01
2276	70.93	2280	73.93	2270	71.89
2379	70.83	2383	73.87	2373	71.78
2483	70.74	2486	73.82	2476	71.68
2586	70.67	2589	73.77	2579	71.61
2689	70.62	2693	73.73	2682	71.51
2791	70.58	2796	73.69	2785	71.46
2895	70.54	2900	73.65	2888	71.41
2998	70.51	3003	73.62	2992	71.36
3101	70.48	3106	73.59	3095	71.32
3204	70.46	3210	73.56		
3307	70.44	3313	73.54		

C.2. Apparent degree of reduction achieved illustrations (I)

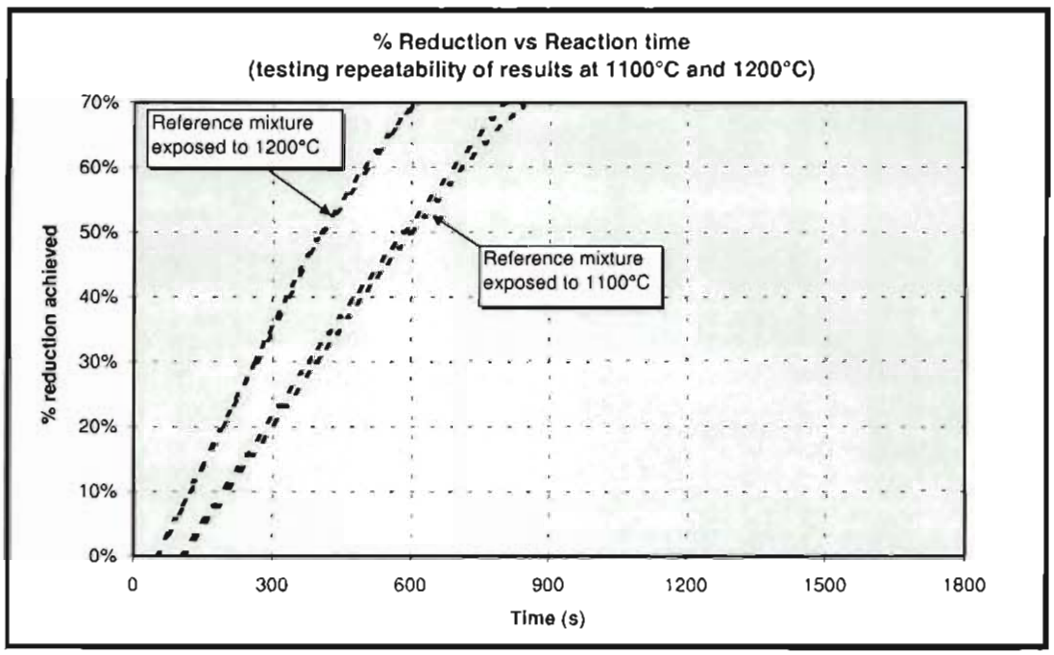

***Figure C 1**: Reduction rate of two runs with the base mixture exposure to 1100°C and two runs with the base mixture exposure to 1200°C, showing the repeatability of results.*

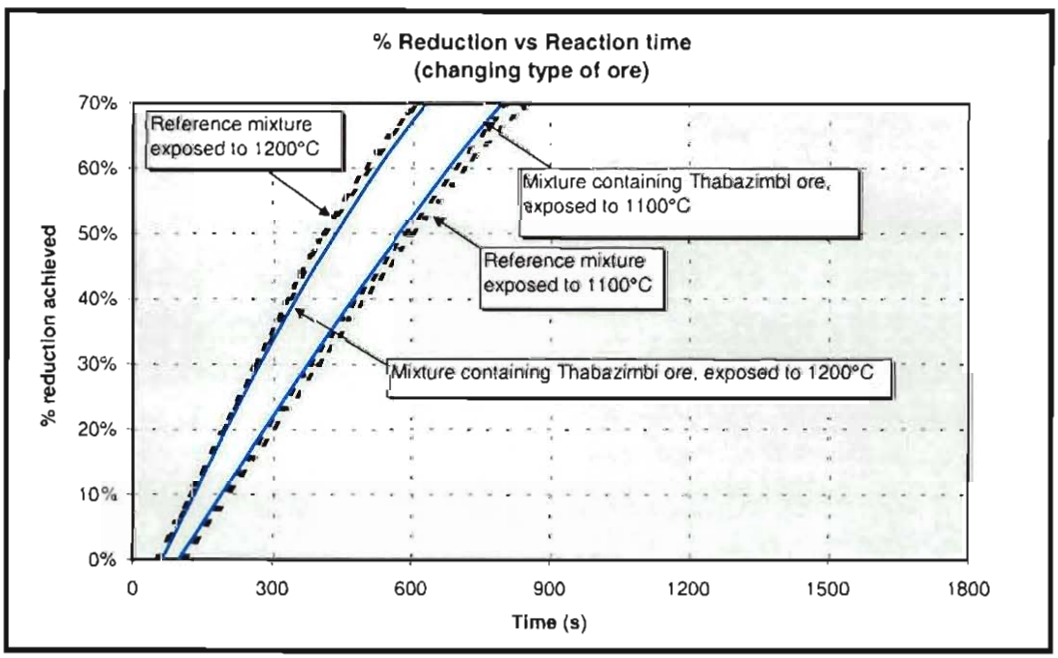

***Figure C 2**: Reduction rate of base mixture and a mixture contalning Thabazimbi fine ore exposed to 1100°C and 1200°C.*

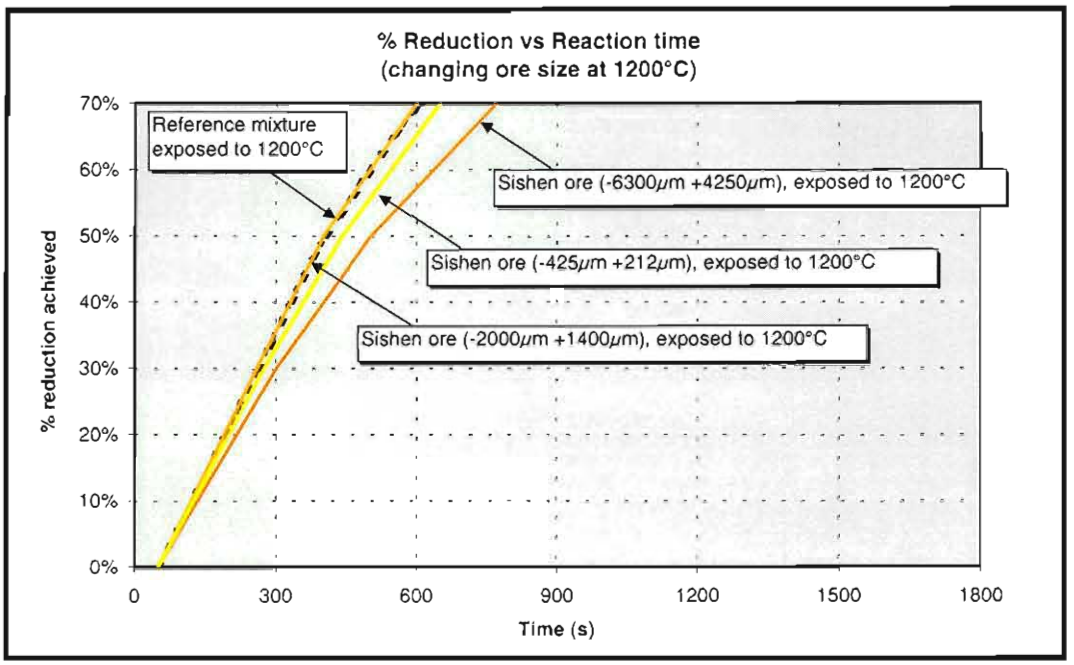

***Figure C 3**: Reduction rate of base mixture and a mixture containing various size fractions of Sishen ore during exposure to 1200°C.*

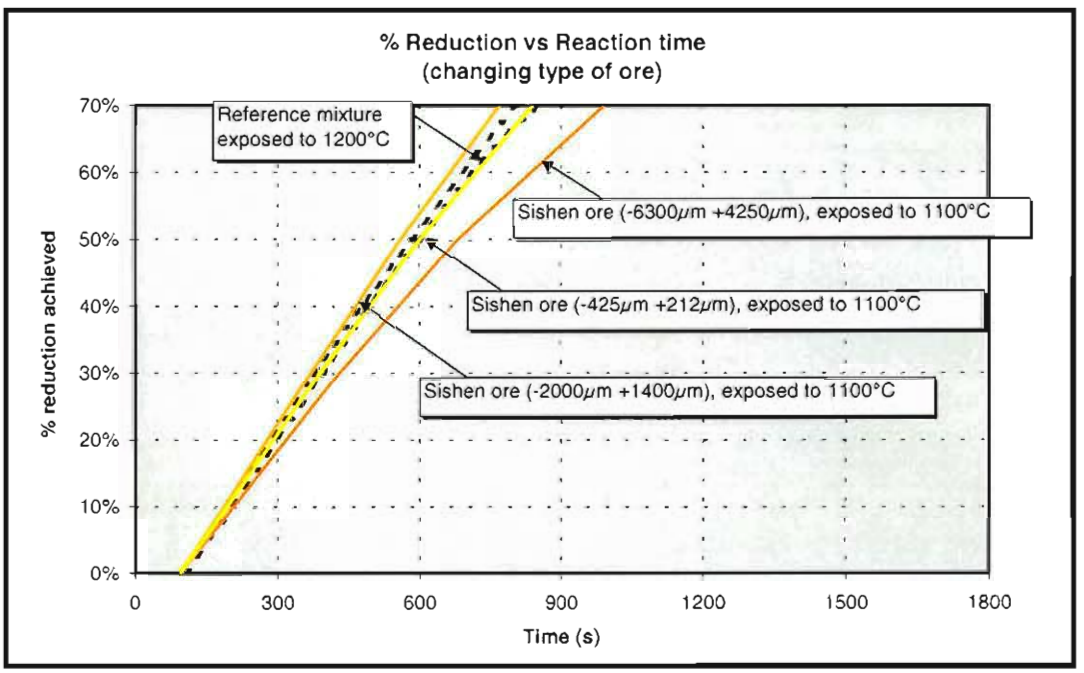

***Figure C 4**: Reduction rate of base mixture and a mixture containing various size fractions of Sishen ore during exposure to 1100°C.*

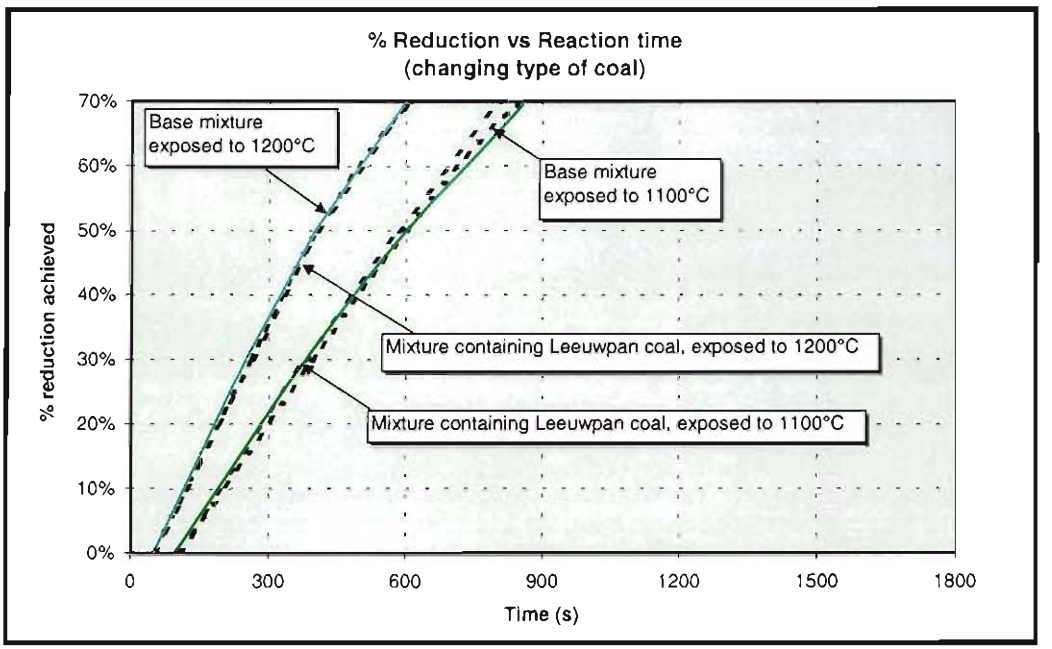

***Figure C 5**: Reduction rate of base mixture and a mixture containing Leeuwpan coal exposed to 1100°C and 1200°C.*

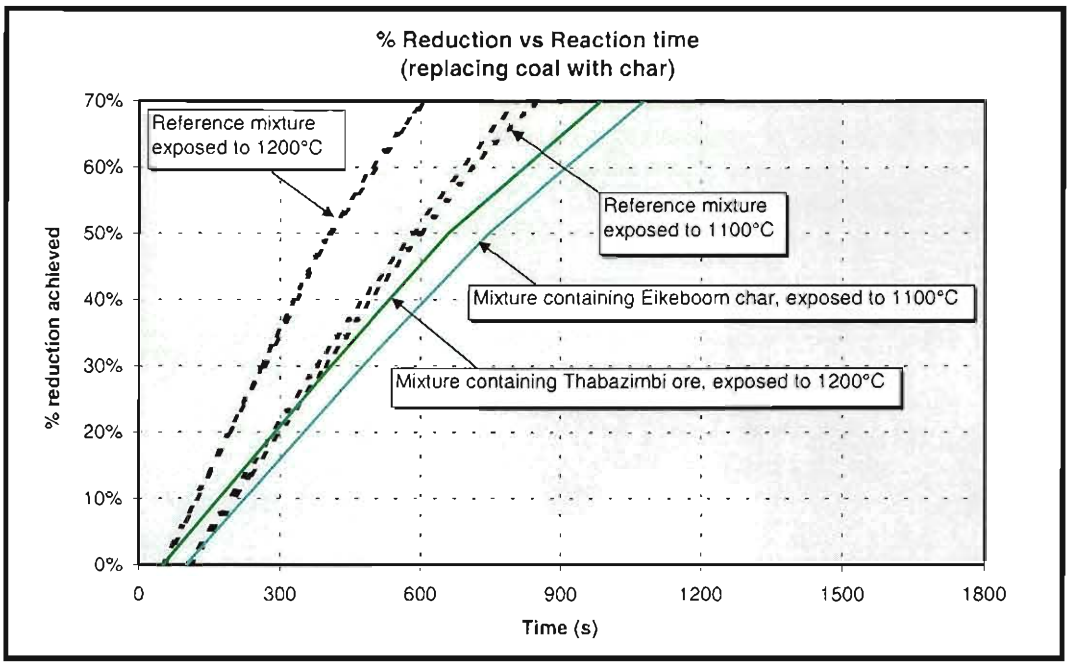

***Figure C 6**: Reduction rate of base mixture and a mixture containing Thabazimbi fine ore exposed to 1100°C and 1200°C.*

Figures C 1 to ***C6*** show the apparent degree of reduction achieved calculated according to the procedure presented in ***Appendix A.7***. The figures show that reduction only started after approximately 2 minutes. This is a result of the assumption that calcinations of $MgCO_3$ is completed before reduction starts. However the results support the findings of ***paragraph 2.4***. These calculations were based on the assumption that volatiles contribute to the reduction reaction and that both CO and CO_2 formed as reduction products. The CO/CO_2 ratio of the product gas was calculated as the CO/CO_2 in equilibrium with iron oxide. This is the one limit regarding the extent of reduction achieved.

The other limit is when calculations are based on the assumption that volatiles do not contribute to reduction and only CO forms as gaseous product (due to reduction). The results when using this approach are presented in ***Figures C 7***to ***C 12*** in ***Appendix C.3.***

C.3. Apparent degree of reduction achieved illustrations (II)

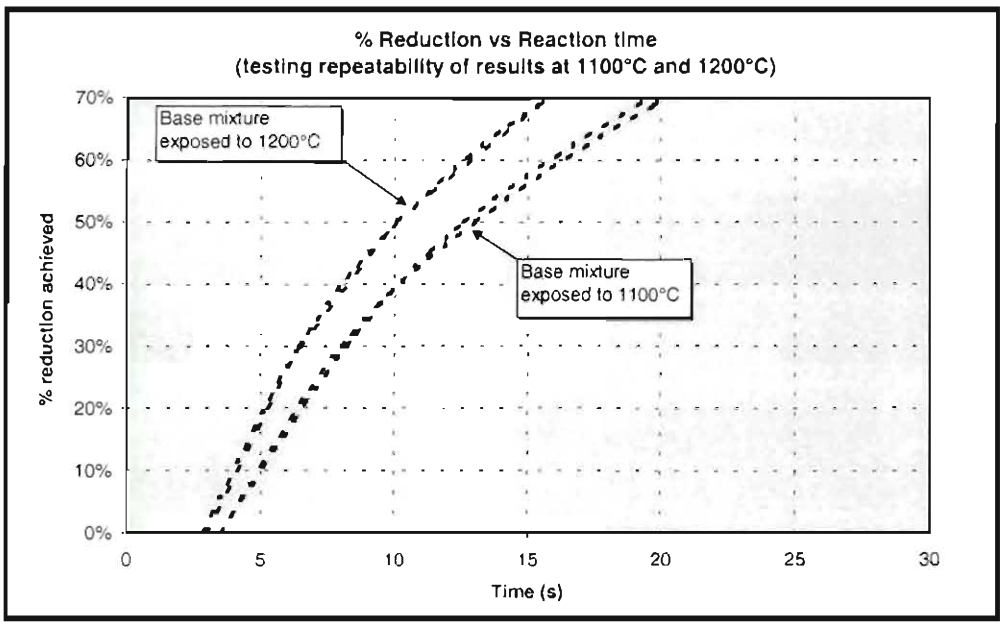

***Figure C 7**: Reduction rate of two runs with the base mixture exposure to 1100°C and two runs with the base mixture exposure to 1200°C, showing the repeatability of results.*

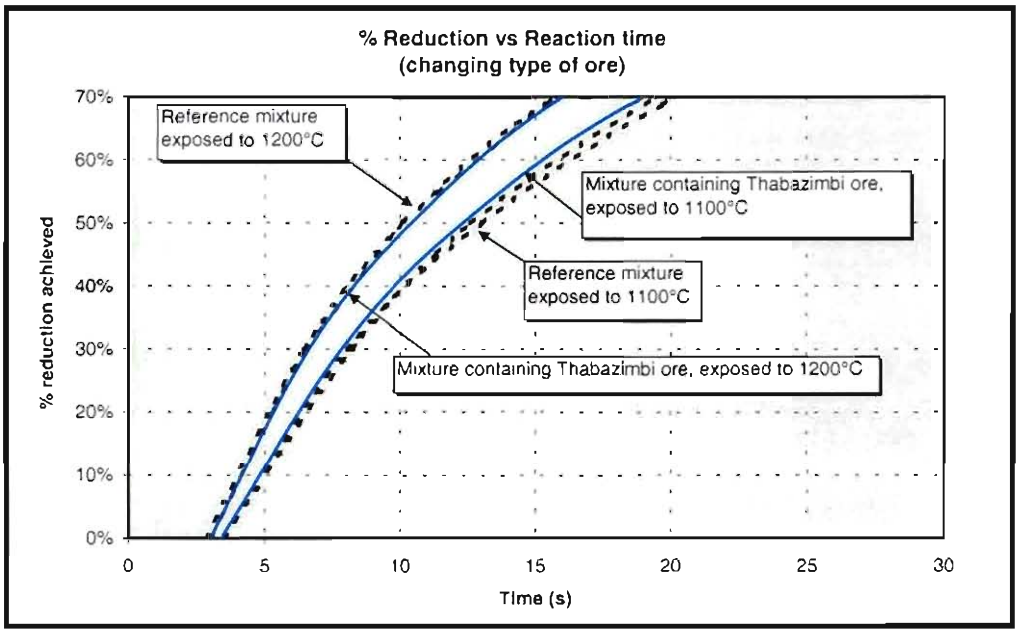

***Figure C 8**: Reduction rate of base mixture and a mixture containing Thabazimbi fine ore exposed to 1100°C and 1200°C.*

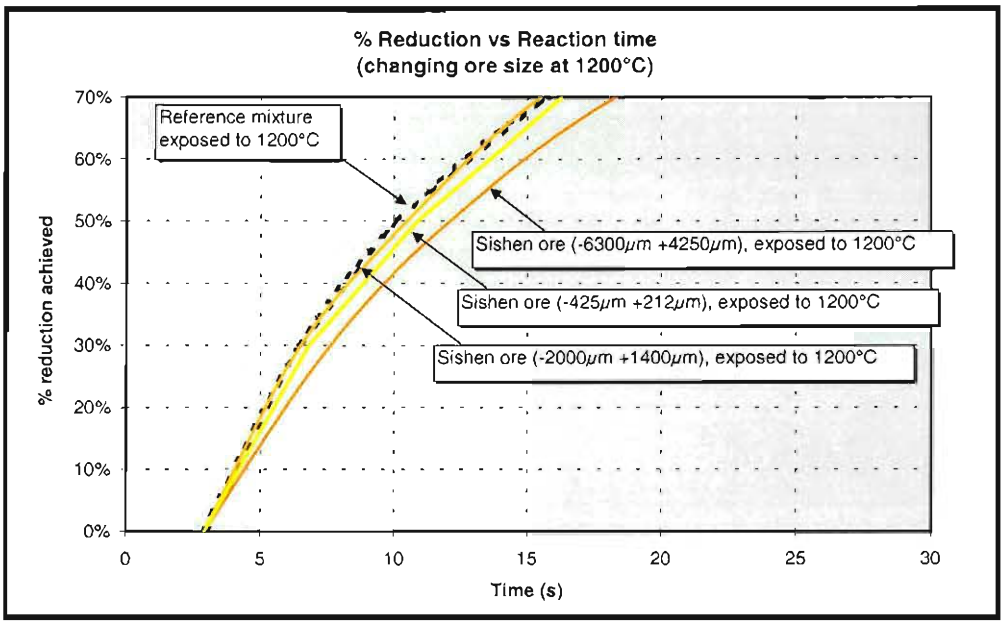

***Figure C 9**: Reduction rate of base mixture and a mixture containing various size fractions of Sishen ore during exposure to 1200°C.*

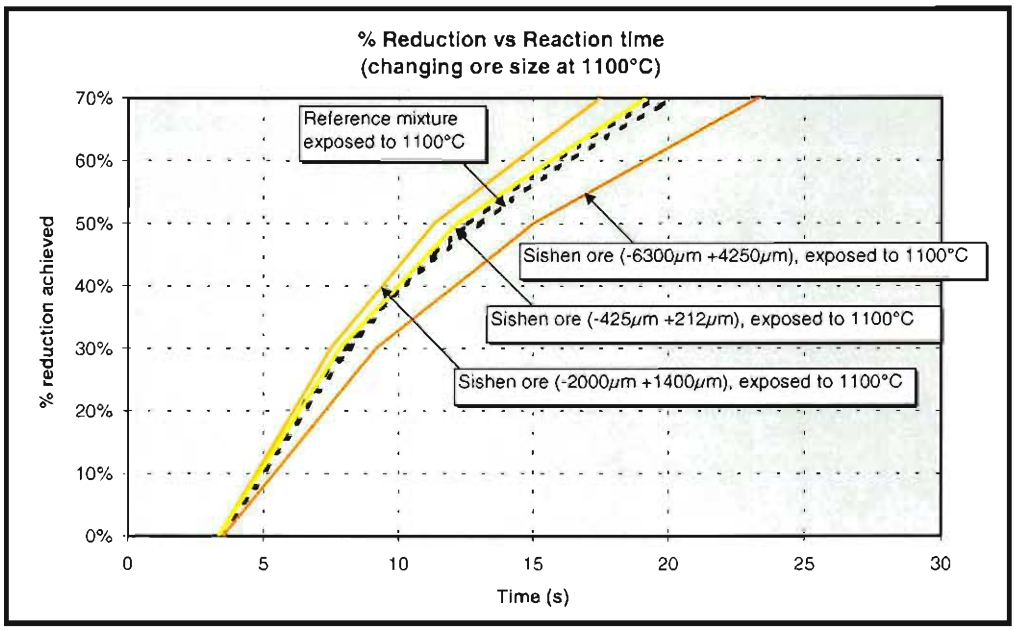

***Figure C 10**:Reduction rate of base mixture and a mixture containing various size fractions of Sishen ore during exposure to 1100°C.*

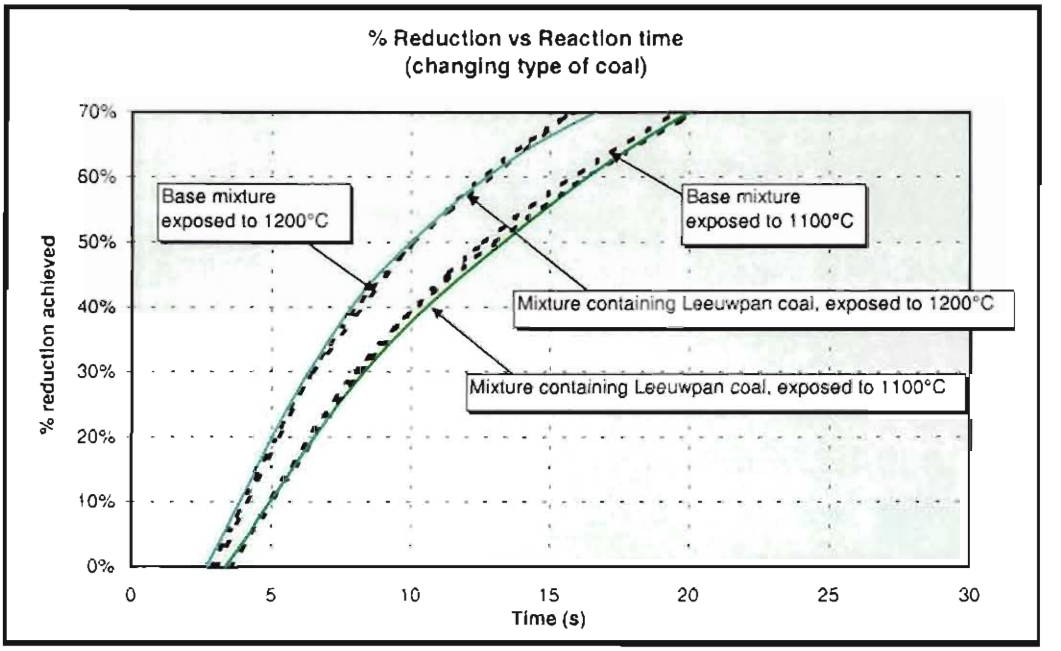

***Figure C 11**: Reduction rate of base mixture and a mixture containing Leeuwpan coal exposed to 1100°C and 1200°C.*

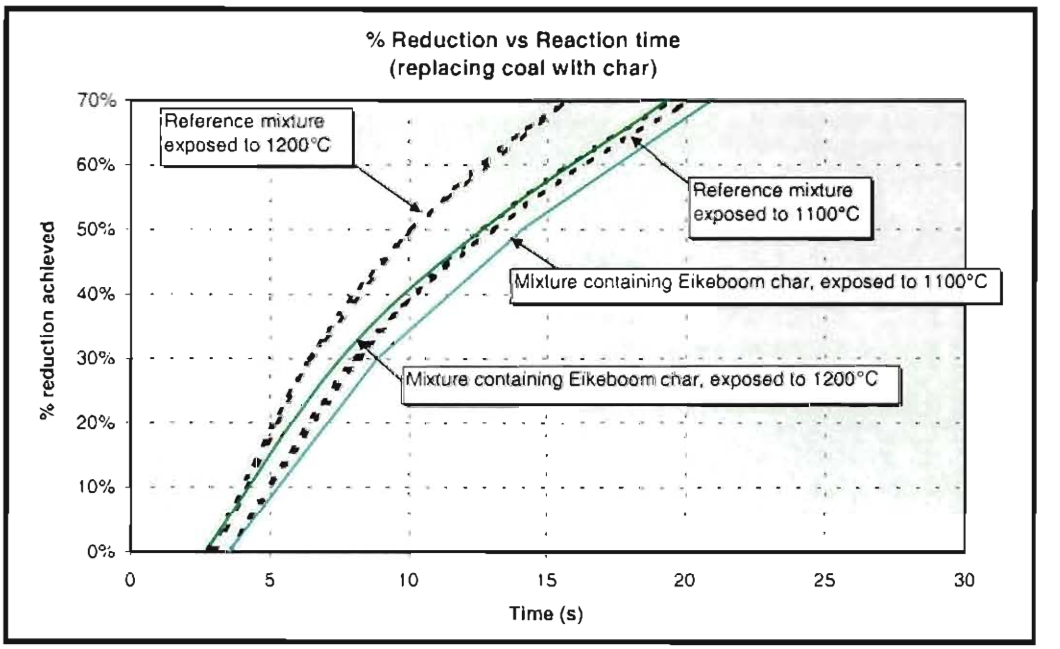

***Figure C 12**: Reduction rate of base mixture and a mixture containing Thabazimbi fine ore exposed to 1100°C and 1200°C.*

The results that are shown in ***Figures C 7*** to ***C12*** show the apparent degree of reduction achieved calculated according to the procedure presented in ***Appendix A.7.*** These calculations were based on the assumption that volatiles did not contribute to the reduction reaction and that only CO formed as reduction products.

The results shown in ***Appendix C.2*** and ***Appendix C.3*** complimented each other , and confirmed results presented from ***paragraph 2.4***. Note that the time before reduction starts is longer when reduction by volatiles are not accounted for, since the initial mass loss accounts for calcinations of $MgCO_3$ and loss of volatiles (without reduction occurring). It should therefore be kept in mind that the results presented in ***Appendix C.2*** and ***Appendix C.3*** are not fundamental reduction rates but rather apparent reduction rates based on specific sets of assumptions.

APPENDIX D

Reaction kinetics

Page no

D.1 Calculation of gas flow rates to overcome mass transfer control

For the fluidization tests, flow rates were selected according to the following requirements[30]

- The flow rate must be at least equal to the minimum flow rate required for fluidisation.
- The minimum fluidisation flow rate should be less than 12 l/min (due to equipment restrictions).
- The mass transfer constant for fluidisation must be at least 10 times the chemical reaction rate constant at the experimental temperature.

D.1.1 Calculation of required flow rate for fluidisation

The minimum fluidisation velocity required for each size fraction at the experimental temperature was calculated using the following equation:[30]

$$u_{mf} = \left[\left((33.7)^2 + 0.0408 \frac{d_p^3 \rho_g (\rho_s - \rho_g) g}{\mu^2} \right)^{1/2} - 33.7 \right] \cdot \frac{\mu}{d_p \rho_g} \qquad \text{(D.a)}$$

where u_{mf} *is the* minimum fluidisation velocity (with unit: m/s), ρ_s is the solids density (with unit: kg/m^3), ρ_g is the gas density (with units: kg/m^3), μ is the gas viscosity (with units: kg/ms), d_p is the particle diameter (with unit: m), g is gravitational acceleration (9.81 m/s^2), k_d is the gas phase mass transfer coefficient (with units: m/s), $D_{A\text{-}B}$ is the binary diffusivity of A in B (with units: m/s^2), Re is the Reynolds number, Sc is the Schmidt number, and Sh is the Sherwood number.

The diffusivity in the binary gas systems was calculated as follows:

$$D_{A-B} = \left(\frac{(1\times10^{-3})T^{1.75}}{P(v_B^{1/3} + v_A^{1/3})^2} \left[\frac{1}{M_A} + \frac{1}{M_B} \right]^{1/2} \right) \times \frac{1}{100} \qquad \text{(D.b)}$$

Where T is temperature (with unit: K), P is pressure (0.86 atm),v_A is the diffusion volume of specie A (with unit: m^3) and M_A is the molecular weight of specie A (with unit: g/mol).

The gas phase mass transfer coefficient was calculated as follows:

$$\mathrm{Re} = \frac{d_p \rho_g u_{mf}}{\mu} \qquad \text{(D.c)}$$

The Reynolds number and Schmidt numbers were used to calculate the Sherwood number from the following equations:

$$Sc = \frac{\mu}{\rho_g D_{A-B}}$$

For 0.1 < Re >15:

$$Sh = 0.374\mathrm{Re}^{1.2} Sc^{1/3} \qquad \text{(D.d)}$$

For 15 < Re >250:

$$Sh = 2.01\mathrm{Re}^{1.2} Sc^{1/3} \qquad \text{(D.e)}$$

The Sherwood number is then used in the following equation to calculate the gas phase mass transfer coefficient:

$$Sh = \frac{k_d d_p}{D_{A-B}} \qquad \text{(D.f)}$$

For the minimum fluidisation velocity and the reactor diameter of 25 mm a minimum fluidisation flow rate was calculated by multiplying the reactor cross sectional area with the minimum fluidisation gas velocity. The gas phase mass transfer coefficient for the minimum fluidisation velocity was then calculated, and this coefficient was compared to the chemical reaction rate constant. If the gas phase mass transfer coefficient was more than ten times larger than the chemical reaction rate constant, the experimental gas flow was assumed sufficient to overcome gas phase mass transfer control.

Only small particle were fluidised. Calculations showed that the gas flow rates required to overcome mass transfer control for the large particles were less than the gas flow rate required for fluidisation of the large particles.

The experimental conditions used for determining the rate constant of each size fraction are shown in ***Table D.1*** and ***Table D.2***.

Table D 1: *Experimental conditions for ore Reduction with CO gas at 800°C, 900°C, 950°C and 1000°C*

Size Fraction (μm)	Gas flow rate for 800°C (l/min) @ STD	Gas flow rate for 900°C (l/min) @ STD	Gas flow rate for 950°C (l/min) @ STD	Gas flow rate for 1000°C (l/min) @ STD	Fluidise/Packed bed
-212 +106	0.45	0.39	0.37	0.35	Fluidise
-300 +212	0.74	0.65	0.61	0.58	Fluidise
-850 +425	4.11	3.63	3.42	3.50	Fluidise
-2800 +2000	1.80	1.80	1.80	1.80	Packed
-6300 +4750	1.80	1.80	1.80	1.80	Packed

Table D 2: *Experimental conditions for char gasification with CO_2 gas at 800°C, 850°C, 900°C, and 950°C.*

Size Fraction (μm)	Gas flow rate for 800°C (l/min) @ STD	Gas flow rate for 850°C (l/min) @ STD	Gas flow rate for 900°C (l/min) @ STD	Gas flow rate for 950°C (l/min) @ STD	Fluidise/Packed bed
-212 +106	0.1	0.1	0.1	0.1	Fluidise
-425 +212	0.5	0.4	0.4	0.4	Fluidise
-850 +425	1.8	1.7	1.6	1.5	Fluidise
-2000 +1400	7.8	7.5	7.1	6.8	Fluidise

D.1.2 Determining of required flow rate for packed bed

For the packed bed experiments, the required flow rate had to be determined experimentally. For this, reduction tests were repeated at the maximum temperature (1000°C) and the flow rate was increased during each test. The minimum flow rate for which the reduction/gasification rate became independent of gas flow rate was the minimum flow rate that was used for the specific set of experiments. This gas flow rate was then used for all of the experiments in the particular size fraction material. ***Figure D 1*** shows the results of the above procedure done for CO reducibility of the ore.

Figure D 1: *Minimum CO flow rate required for iron ore reducibility tests – Stagnant bed*

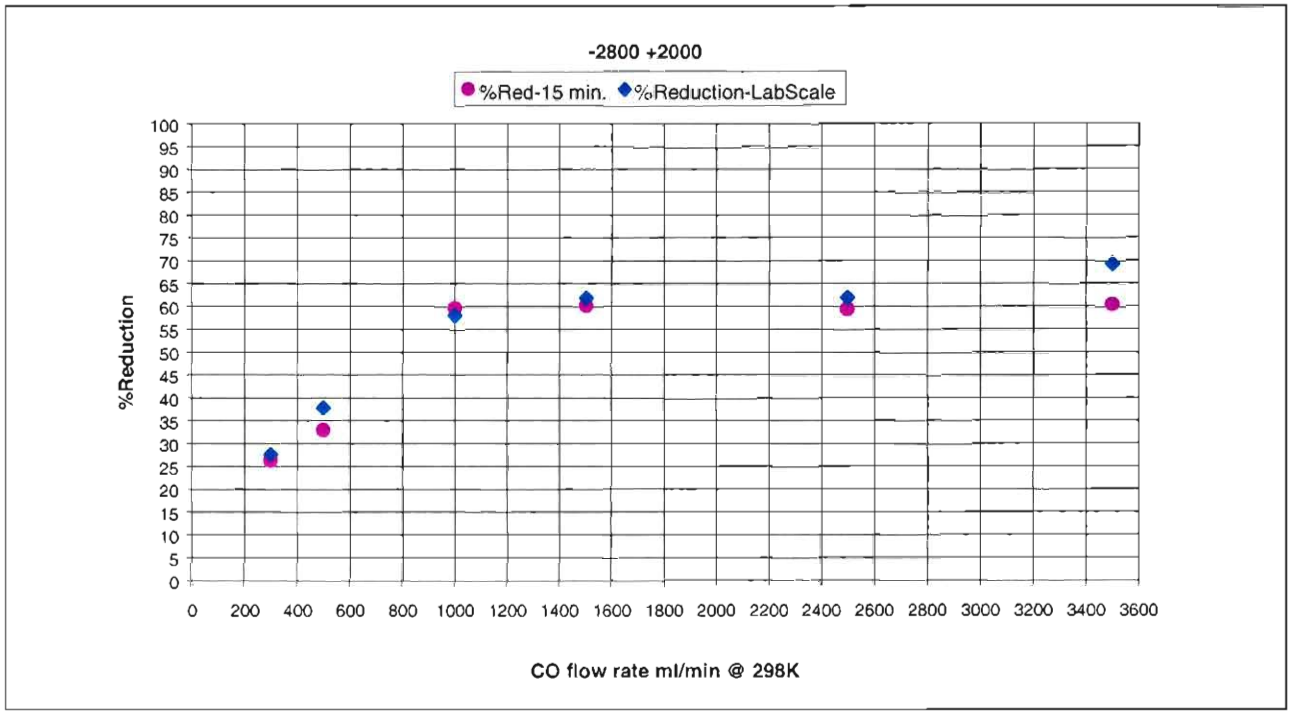

D.2 Summary of kinetic data

This paragraph presents the raw experimental data of the kinetic study.

***Table D.1**: Kinetic data for reduction of -212 +106 µm Sishen ore particles with CO gas.*

900	°C	950	°C	1000	°C
Time (s)	Mass (g)	Time (s)	Mass (g)	Time (s)	Mass (g)
-117	5.766	-150	5.718	-75	5.616
33	5.656	0	5.718	75	5.376
183	5.306	150	5.378	225	4.936
333	4.976	300	5.028	375	4.606
483	4.696	450	4.728	525	4.326
633	4.446	600	4.448	675	4.066
782	4.246	750	4.208	825	3.876
932	4.106	900	4.038	974	3.726
1082	3.976	1050	3.888	1124	3.606
1232	3.856	1200	3.758	1274	3.486
1382	3.746	1350	3.648	1424	3.396
1532	3.646	1500	3.538	1574	3.276
1682	3.566			1724	3.196
1832	3.456				
1982	3.336				
2132	3.246				
2282	3.166				

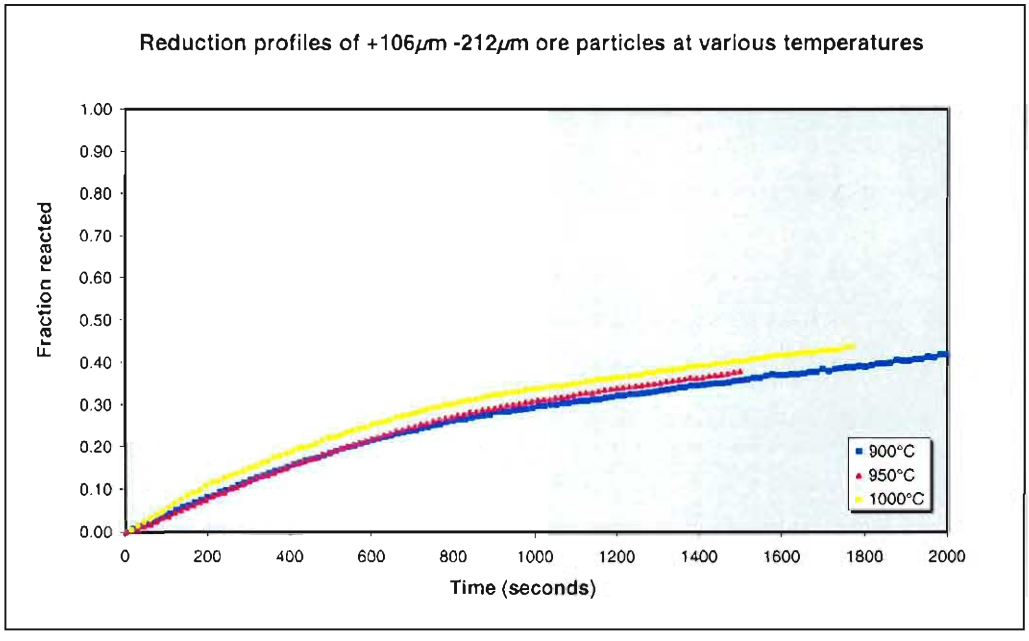

***Figure D 2:** Fraction of reducible oxygen removed as a function of reaction time during reduction of Sishen ore particles (in the size range -212µm +106µm) with CO gas.*

***Table D.2**: Kinetic data for reduction of -300 +212 µm Sishen ore particles with CO gas.*

800	°C	900	°C	950	°C	1000	°C
Time (s)	Mass (g)	Time (s)	Mass (g)	Time (s)	Mass (g)	Time (s)	Mass (g)
15	5.607	105	5.205	0	5.667	3	5.751
165	4.797	255	4.655	150	5.007	153	5.101
315	4.367	405	4.265	300	4.517	303	4.511
465	4.097	555	3.995	450	4.127	453	4.061
615	3.897	705	3.795	600	3.847	602	3.741
765	3.717	855	3.625	750	3.617	752	3.481
915	3.567	1005	3.445	900	3.407	902	3.241
1065	3.397	1155	3.255	1050	3.217	1052	3.001
1215	3.247	1305	3.095	1200	3.027	1202	2.791
1365	3.097	1455	2.945	1350	2.837	1352	2.581
1515	2.957	1605	2.755	1500	2.647	1502	2.381
1665	2.807	1755	2.605	1650	2.467	1652	2.191
1815	2.677	1905	2.475			1802	1.991
1965	2.547	2055	2.315				
2115	2.417	2205	2.155				
2265	2.307	2355	2.025				
		2505	1.905				

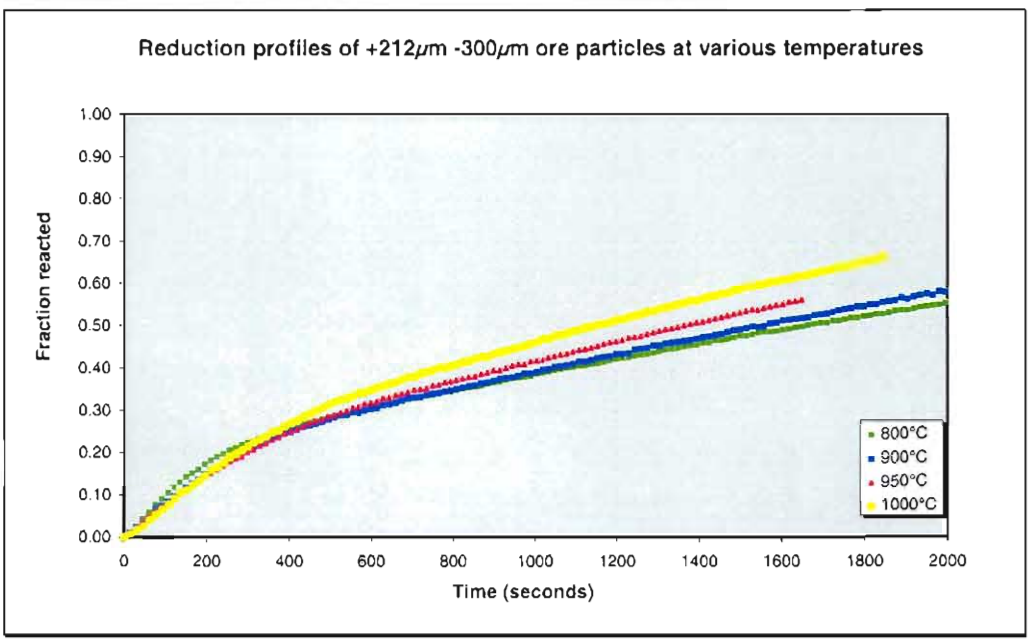

***Figure D 3:** Fraction of reducible oxygen removed as a function of reaction time during reduction of Sishen ore particles (in the size range -300µm +212µm) with CO gas.*

***Table D.3**: Kinetic data for reduction of –850 +425 µm Sishen ore particles with CO gas.*

850	°C	950	°C	1000	°C
Time (s)	Mass (g)	Time (s)	Mass (g)	Time (s)	Mass (g)
0	5.653	90	4.871	59	5.167
50	5.323	240	4.131	209	4.187
100	4.983	390	3.701	359	3.547
150	4.703	540	3.261	509	2.957
200	4.513	690	2.831	659	2.407
250	4.353	840	2.391	809	1.967
300	4.203	990	1.951	959	1.617
350	4.073	1140	1.611	1109	1.397
400	3.963	1290	1.351	1259	1.217
450	3.863	1439	1.171	1409	1.117
500	3.763	1589	1.041	1559	1.047
550	3.683	1739	0.981	1709	0.997
600	3.583			1859	0.957
650	3.513				
700	3.423				
750	3.313				
800	3.263				

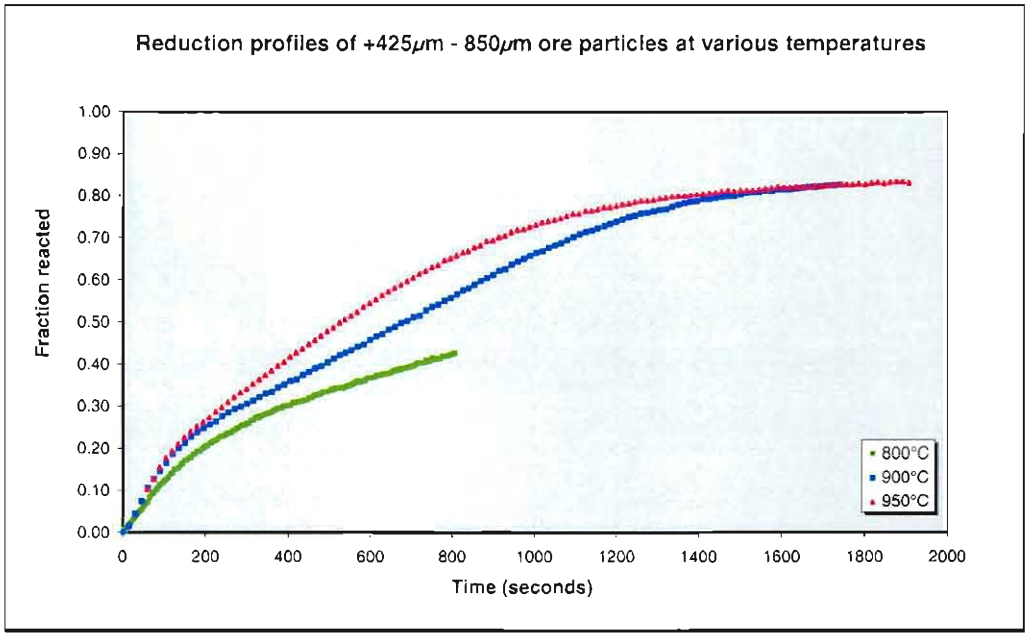

***Figure D 4:** Fraction of reducible oxygen removed as a function of reaction time during reduction of Sishen ore particles (in the size range –850µm +425µm) with CO gas.*

***Table D.4**: Kinetic data for reduction of -2800 +2000 µm Sishen ore particles with CO gas.*

800	°C	850	°C	950	°C
Time (s)	Mass (g)	Time (s)	Mass (g)	Time (s)	Mass (g)
98	5.570	105	5.450	66	5.396
248	5.150	255	4.890	166	4.836
398	4.830	405	4.490	266	4.376
548	4.610	555	4.200	366	3.936
698	4.430	705	3.930	466	3.566
848	4.260	855	3.680	566	3.226
998	4.110	1005	3.410	666	2.926
1148	3.980	1155	3.170	766	2.666
1298	3.850	1305	2.940		
1448	3.720	1455	2.700		
1598	3.580	1605	2.490		
1748	3.440	1755	2.270		
1898	3.360	1905	2.070		

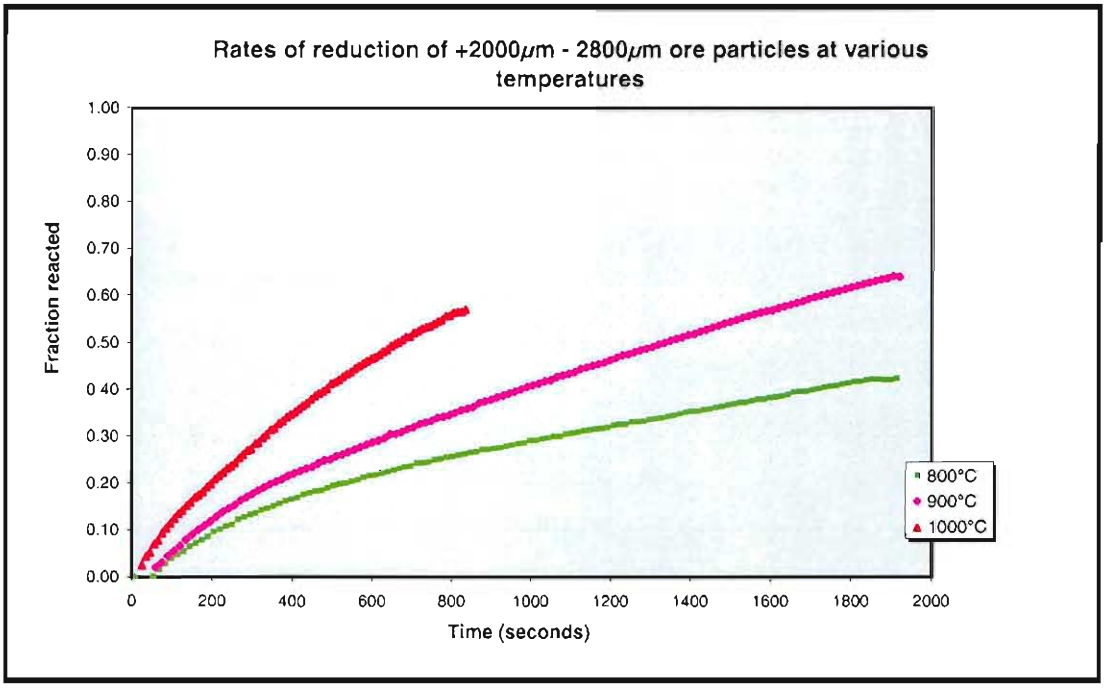

***Figure D 5:** Fraction of reducible oxygen removed as a function of reaction time during reduction of Sishen ore particles (in the size range -2800µm +2000µm) with CO gas.*

***Table D.5**: Kinetic data for reduction of –6300 +4750 µm Sishen ore particles with CO gas*

800	°C	850	°C	950	°C	1000	°C
Time (s)	Mass (g)	Time (s)	Mass (g)	Time (s)	Mass (g)	Time (s)	Mass (g)
95	5.537	75	5.717	90	5.416	75	5.427
245	5.117	225	5.317	240	4.696	225	4.687
394	4.827	375	4.977	390	4.196	375	4.157
544	4.557	525	4.587	540	3.786	525	3.707
694	4.327	675	4.337	690	3.416	675	3.257
844	4.117	825	4.197	840	3.086	825	2.837
994	3.927	975	3.967	990	2.766		
1144	3.777	1125	3.737	1140	2.496		
1294	3.607	1275	3.527	1290	2.226		
1444	3.447	1425	3.377	1440	2.006		
1594	3.307	1575	3.127	1590	1.736		
1744	3.167	1725	3.017	1740	1.536		
1894	3.027	1875	2.807	1890	1.366		
2044	2.907	2025	2.637	2040	1.226		
2194	2.787	2175	2.497	2190	1.056		
2344	2.667	2325	2.407	2340	0.926		
		2475	2.207	2490	0.786		
		2625	2.087	2640	0.696		
		2775	1.967	2790	0.596		
		2925	1.807	2940	0.526		
		3075	1.647	3090	0.446		
		3225	1.547	3240	0.436		
		3375	1.437	3390	0.366		
		3525	1.397	3540	0.336		
		3675	1.297	3690	0.276		

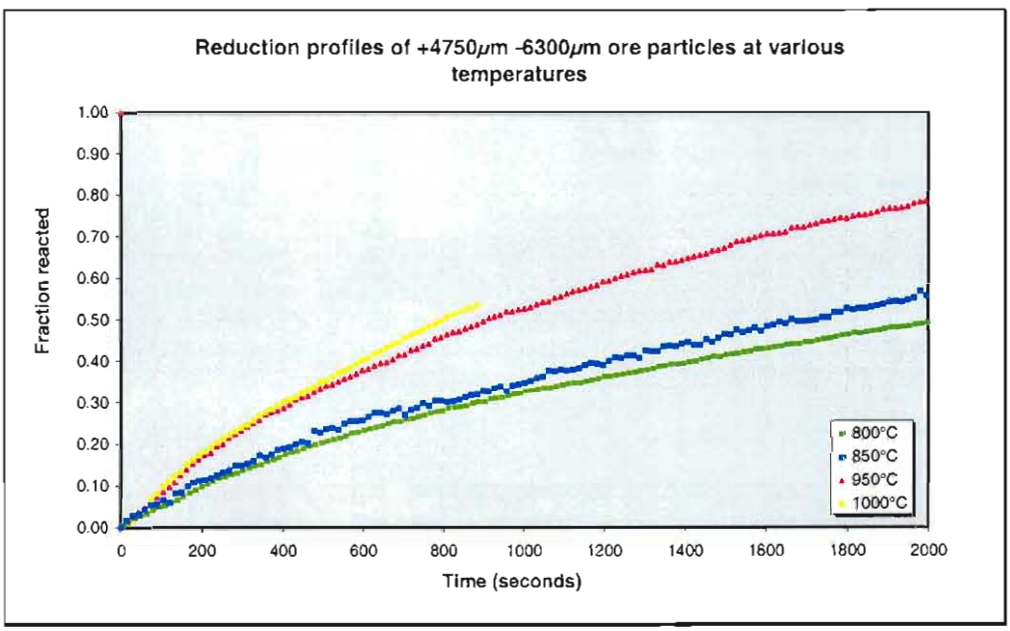

***Figure D 6:** Fraction of reducible oxygen removed as a function of reaction time during reduction of Sishen ore particles (in the size range –6300µm +4750µm) with CO gas.*

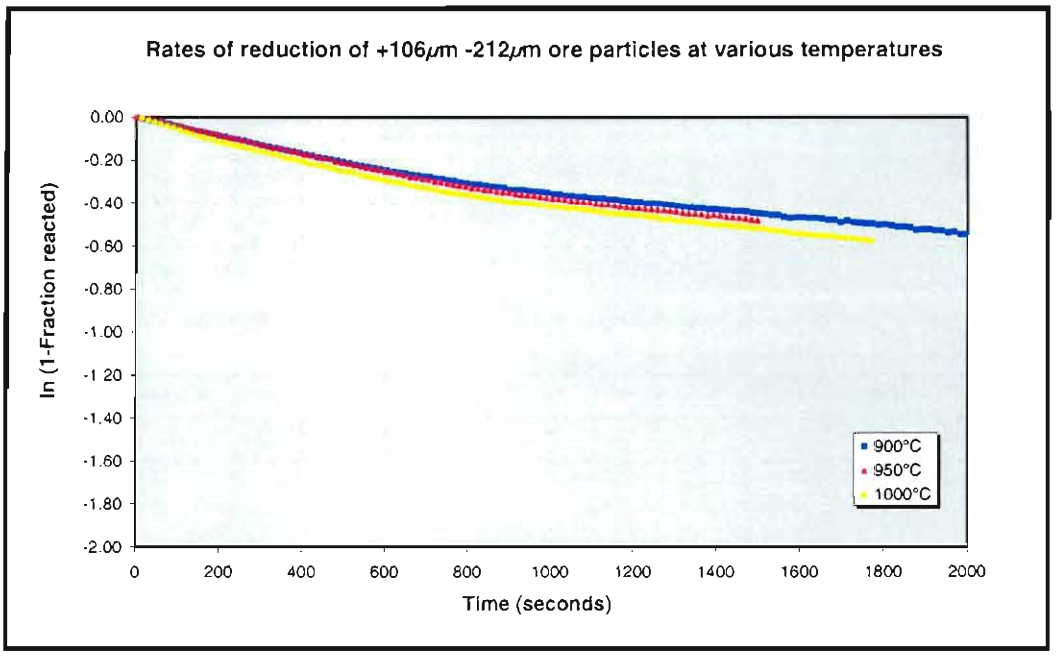

Figure D 2: *ln (1-Fraction of reducible oxygen removed) as a function of reaction time during reduction of Sishen ore particles (in the size range –212μm +106μm) with CO gas.*

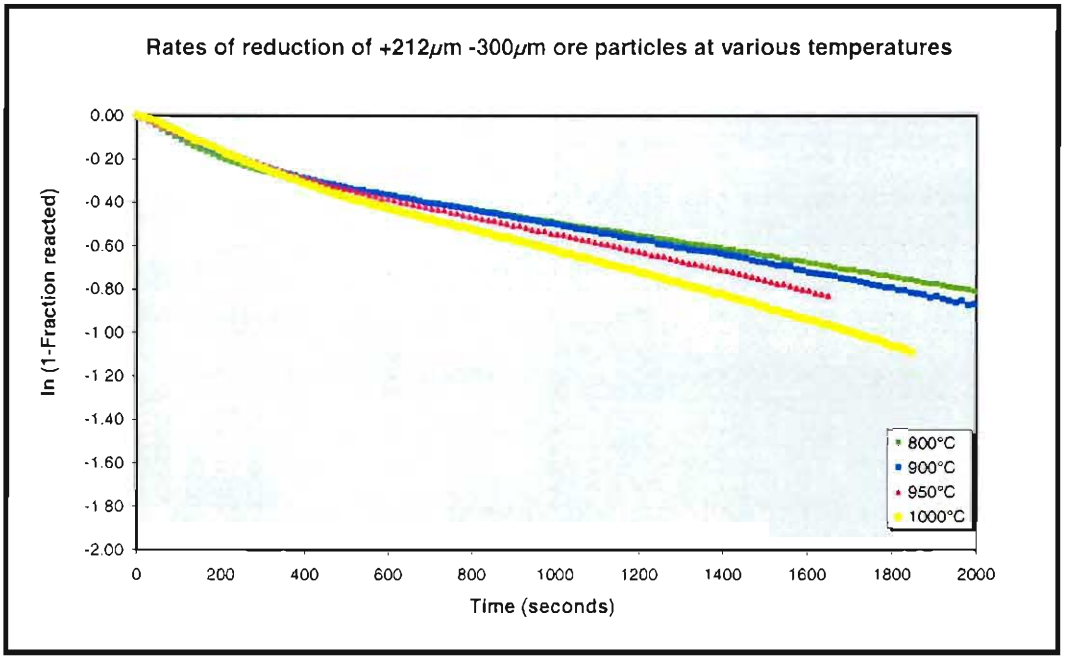

Figure D 3: *ln (1-Fraction of reducible oxygen removed) as a function of reaction time during reduction of Sishen ore particles (in the size range –300μm +212μm) with CO gas.*

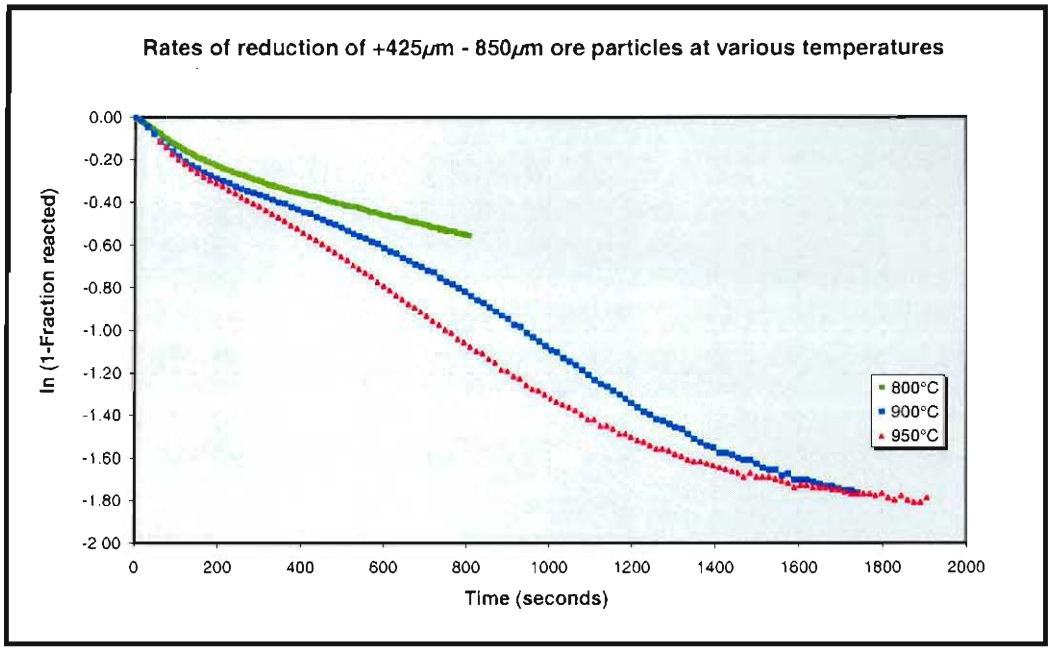

Figure D 4: *ln (1-Fraction of reducible oxygen removed) as a function of reaction time during reduction of Sishen ore particles (in the size range –850μm +425μm) with CO gas.*

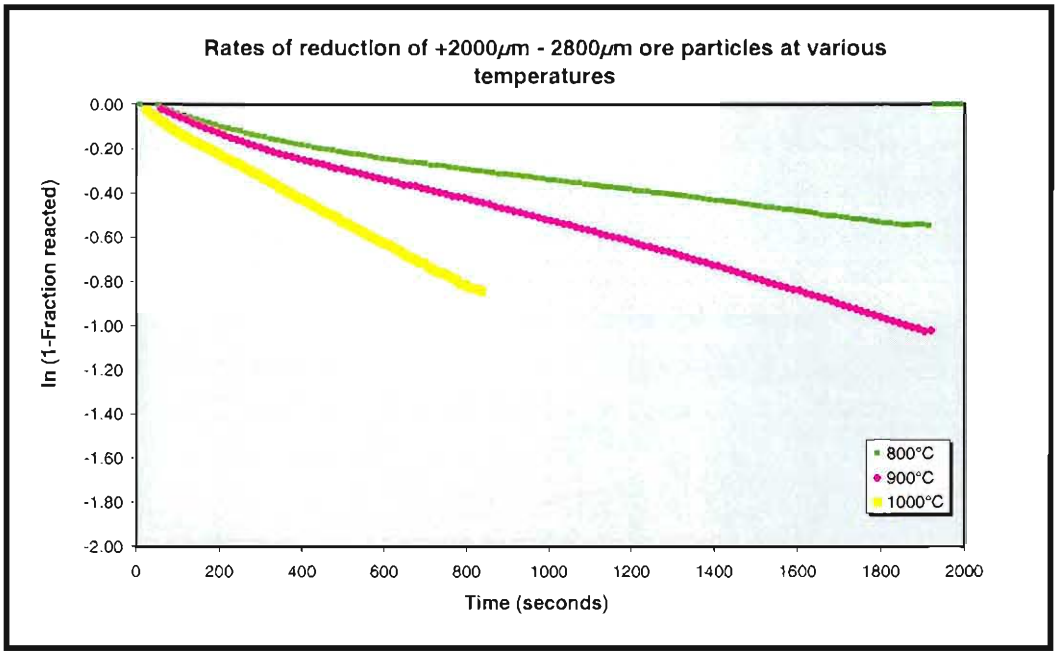

Figure D 5: *ln (1-Fraction of reducible oxygen removed) as a function of reaction time during reduction of Sishen ore particles (in the size range –2800μm +2000μm) with CO gas.*

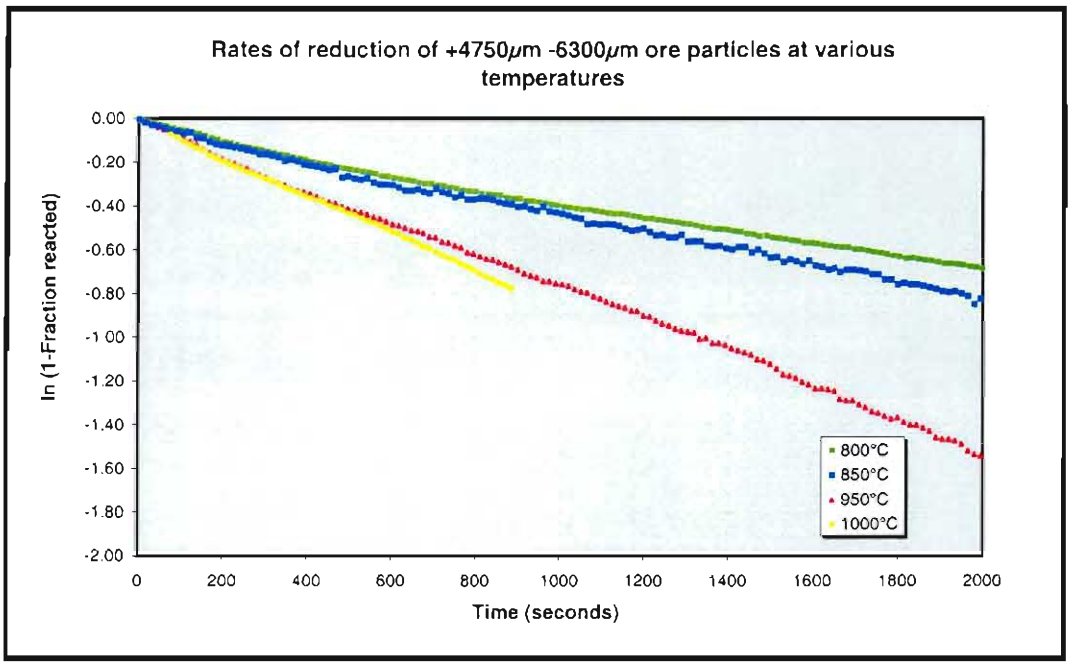

Figure D 6: *Fraction of reducible oxygen removed as a function of reaction time during reduction of Sishen ore particles (in the size range –6300μm +4750μm) with CO gas.*

D.3 Calculation of rate constant and activation energy

Table D.6: *List of rate constants and activation energies calculated from experimental data for degrees of reduction between 0% and 30%.*

0 to 30% reduction

Values of k_{CO}

Particle size range	1/Temperature				
	0.00093	0.00089	0.00085	0.00082	0.00079
+106 -212			9.2E-04	1.1E-03	1.3E-03
+212 -300	1.63E-03		1.8E-03	1.9E-03	2.0E-03
+425-850	2.17E-03		3.2E-03	3.7E-03	
+2000-2800	7.4E-04	1.5E-03		2.9E-03	3.0E-03
+4750-6300	9.6E-04	1.3E-03		2.1E-03	2.6E-03

Values of ln k_{CO}

Particle size range	1/Temperature				
	0.00093	0.00089	0.00085	0.00082	0.00079
+106 -212			-6.99	-6.79	-6.62
+212 -300	-6.42		-6.30	-6.25	-6.19
+425-850	-6.14		-5.76	-5.59	0.00
+2000-2800	-7.21		0.00		-5.81
+4750-6300	-6.95	-6.66		-6.16	-5.94

Interpolated values for ln k_{CO}

Particle size range	1/Temperature				
	0.00093	0.00089	0.00085	0.00082	0.00079
+106 -212	-7.424	-7.195	-6.986	-6.795	-6.617
+212 -300	-6.417	-6.355	-6.299	-6.245	-6.194
+425-850	-6.135	-5.938	-5.759	-5.591	-6.081
+2000-2800	-7.209	-6.494	-6.156	-5.845	-5.805
+4750-6300	-6.948	-6.664	-6.402	-6.161	-5.937

Values of ln k_O and EA

Particle size range	ko (m3/s/kg Fe)	EA (J/mol)
+106 -212	0.10136	45808
+212 -300	0.00676	12667
+425-850	0.00305	3069
+2000-2800	5.61491	79706
+4750-6300	0.59653	57374

Average values for ln k_{CO}

Particle size range	1/Temperature				
	0.00093	0.00089	0.00085	0.00082	0.00079
Average	-6.96104	-6.552775	-6.283238	-6.035427	-5.965703

Average value of ln k_O and EA

	ko (m3/s/kg Fe)	EA (J/mol)
Average	0.53488	56520

Table D.7: *List of rate constants and activation energies calculated from experimental data for degrees of reduction achieved between 30% and 80%*

30 to 80% reduction

Values of k_{CO}

Particle size range	1/Temperature				
	0.00093	0.00089	0.00085	0.00082	0.00079
+106 -212			4.9E-04	5.4E-04	5.9E-04
+212 -300	7.28E-04		1.0E-03	1.2E-03	1.3E-03
+425-850	1.18E-03		2.1E-03	2.7E-03	
+2000-2800	4.8E-04	1.3E-03		3.1E-03	3.2E-03
+4750-6300	5.8E-04	8.8E-04		1.8E-03	2.5E-03

Values of ln k_{CO}

Particle size range	1/Temperature				
	0.00093	0.00089	0.00085	0.00082	0.00079
+106 -212			-7.62	-7.53	-7.44
+212 -300	-7.23		-6.90	-6.75	-6.61
+425-850	-6.74		-6.17	-5.92	0.00
+2000-2800	-7.64		0.00	-5.78	-5.74
+4750-6300	-7.46	-7.04		-6.30	-5.97

Interpolated values for ln k_{CO}

Particle size range	1/Temperature				
	0.00093	0.00089	0.00085	0.00082	0.00079
+106 -212	-7.835	-7.722	-7.619	-7.525	-7.437
+212 -300	-7.225	-7.053	-6.895	-6.748	-6.610
+425-850	-6.743	-6.445	-6.174	-5.921	-6.658
+2000-2800	-7.639	-6.657	-6.201	-5.783	-5.743
+4750-6300	-7.457	-7.039	-6.654	-6.300	-5.972

Values of ln k_O and EA

Particle size range	ko (m3/s/kg Fe)	EA (J/mol)
+106 -212	0.00497	22581
+212 -300	0.03647	34920
+425-850	0.00202	4786
+2000-2800	84.22366	107707
+4750-6300	7.35639	84331

Average values for ln k_{CO}

Particle size range	1/Temperature				
	0.00093	0.00089	0.00085	0.00082	0.00079
Average	-7.454789	-6.890574	-6.520834	-6.181013	-6.098804

Average value of ln k_O and EA

	ko (m3/s/kg Fe)	EA (J/mol)
Average	3.24157	77000

From ***Table D.6.*** and ***Table D.7*** it can be seen that the reduction rate varies significantly with particle size. However, no clear correlation was found between the ore particle size and reaction rate. Reaction rate was therefore found independent of particle size, as would be expected for uniform internal reduction.

As shown in Figure 20 and Figure 21, both uniform and shrinking core reduction patterns were observed for large particles. The reduction rate therefore appears to be influenced more by the morphology of the particles (eg. crack formation, porosity, homogeneity, etc.) than by particle size.

D.4 Model predictions vs measured values

The values of the pre-exponential constant (k_o) and the apparent activation energy (E_a) was used to back-calculate the fraction reacted as a function of time. These graphs were compared to the original data to ensure that the calculated results represented experimental data. These comparisons are shown in ***Figure D.7*** to ***Figure D.11.***

These figures show that the experimental results and model predictions yield similar graphs. This implies that model predictions are representative of the experimentally measured data.

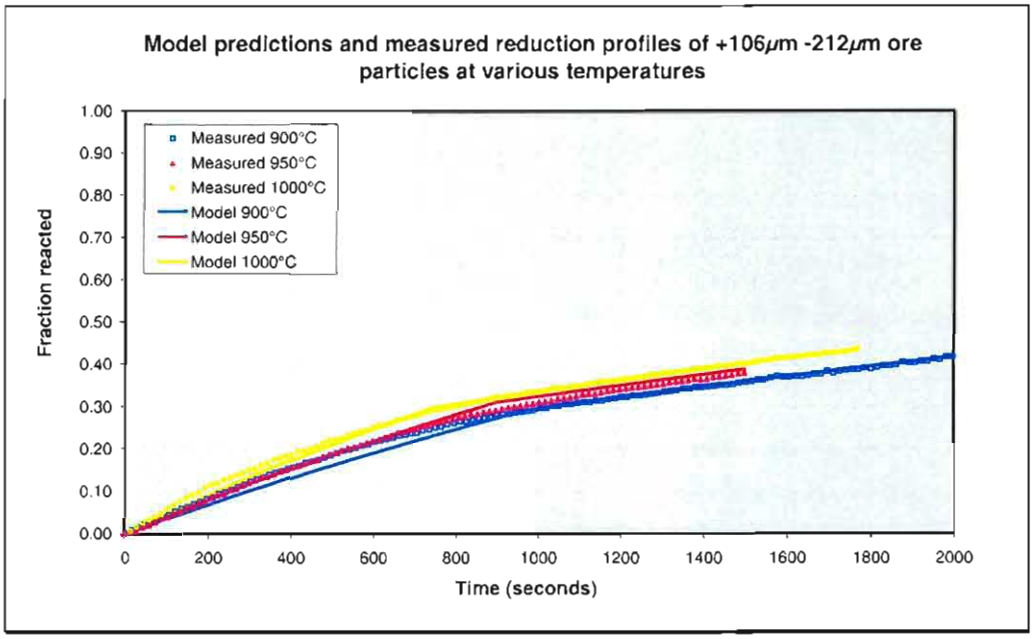

Figure D 7: *Calculated (model) predictions and measured values regarding fraction of reducible oxygen removed as a function of time for ore particles in the size range –212μm +106μm.*

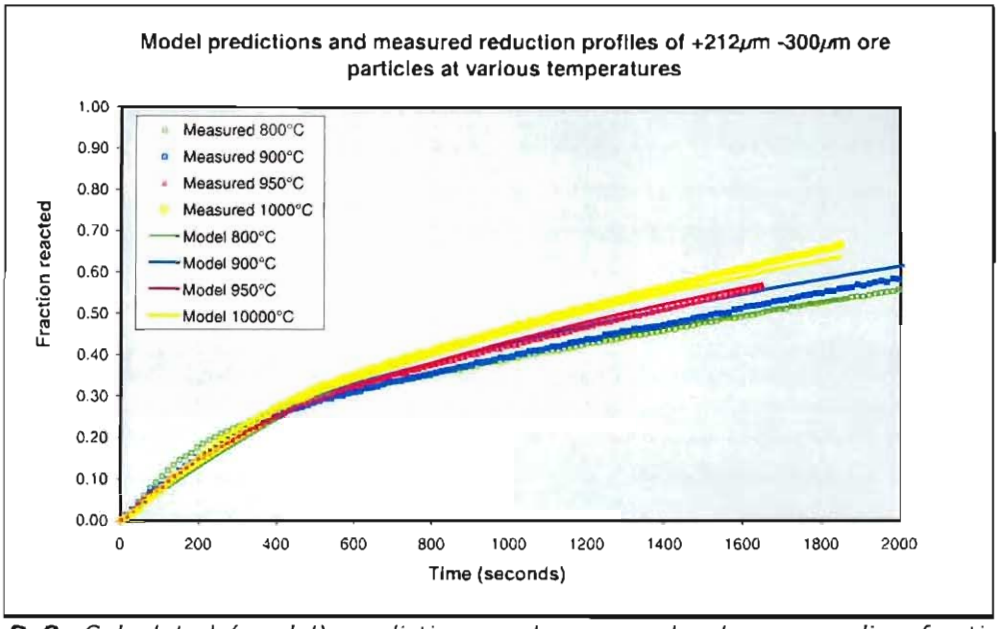

Figure D 8: *Calculated (model) predictions and measured values regarding fraction of reducible oxygen removed as a function of time for ore particles in the size range -300μm +212μm.*

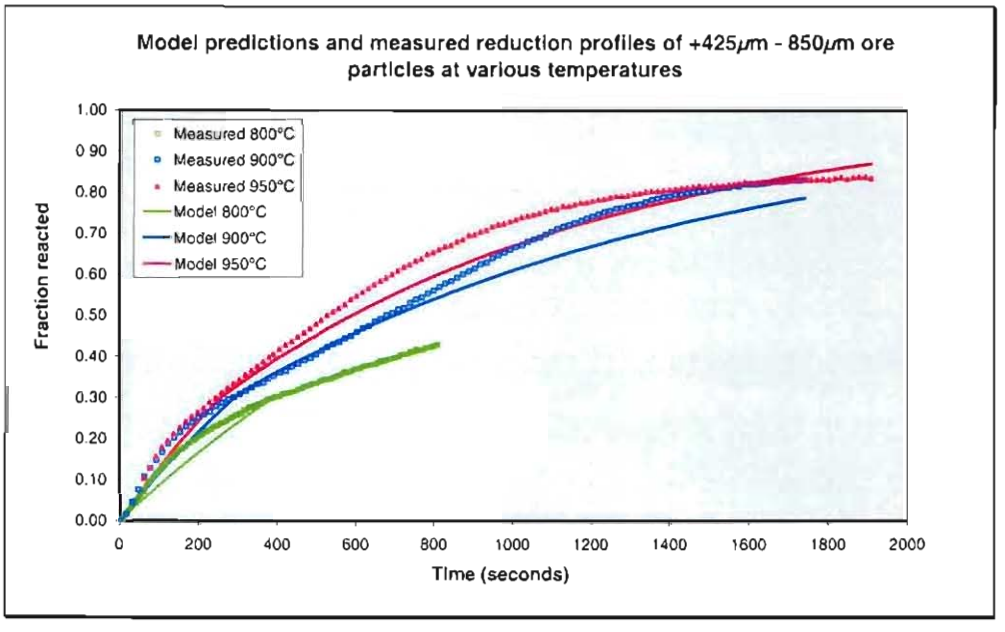

Figure D 9: *Calculated (model) predictions and measured values regarding fraction of reducible oxygen removed as a function of time for ore particles in the size range -850μm +425μm.*

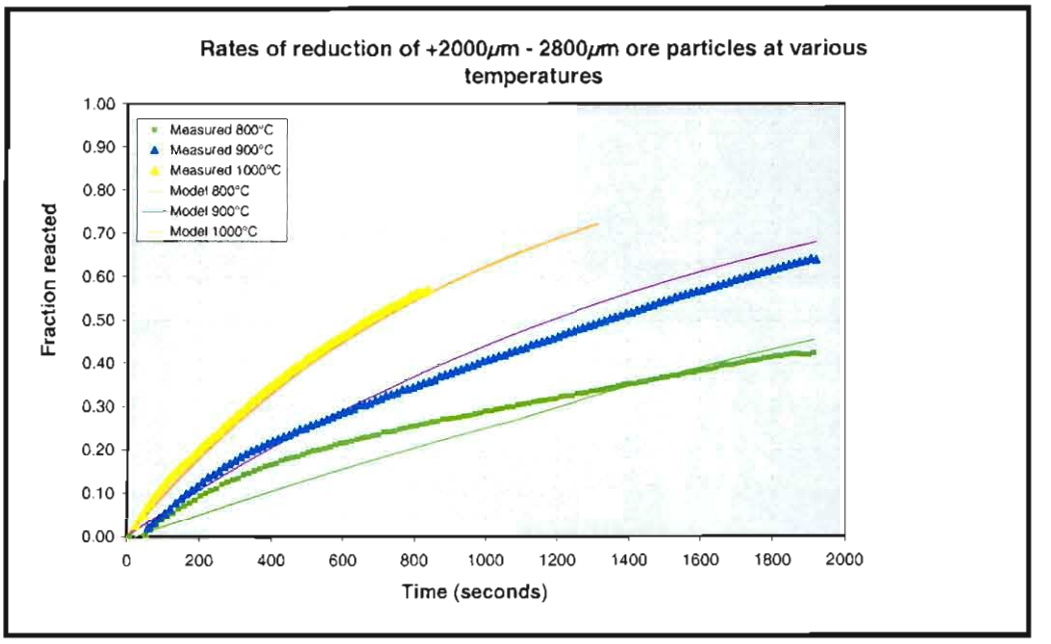

Figure D 10: *Calculated (model) predictions and measured values regarding fraction of reducible oxygen removed as a function of time for ore particles in the size range – 2800μm +2000μm.*

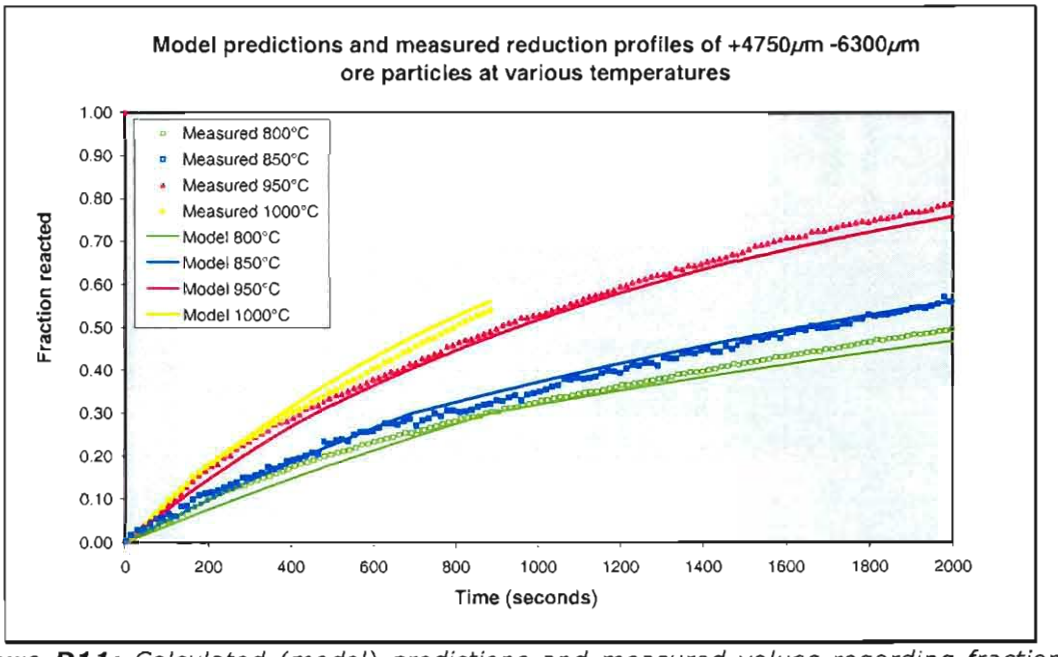

Figure D11: *Calculated (model) predictions and measured values regarding fraction of reducible oxygen removed as a function of time for ore particles in the size range - 6300μm +4750μm.*

APPENDIX E

Model predictions regarding reduction- and temperature profile through the solids bed

E.1 Change in rate constant for the reduction reaction

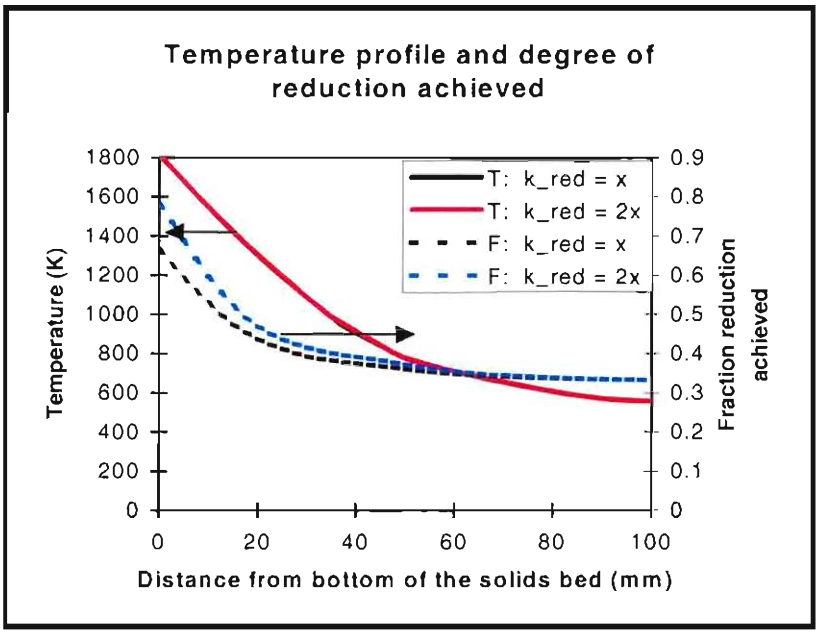

***Figure E 1**: Theoretical profiles of temperature and fraction reduction achieved through a 100mm high solids bed, for a production rate of 30kg/m^2/h, when doubling the rate constant for the reduction reaction.*

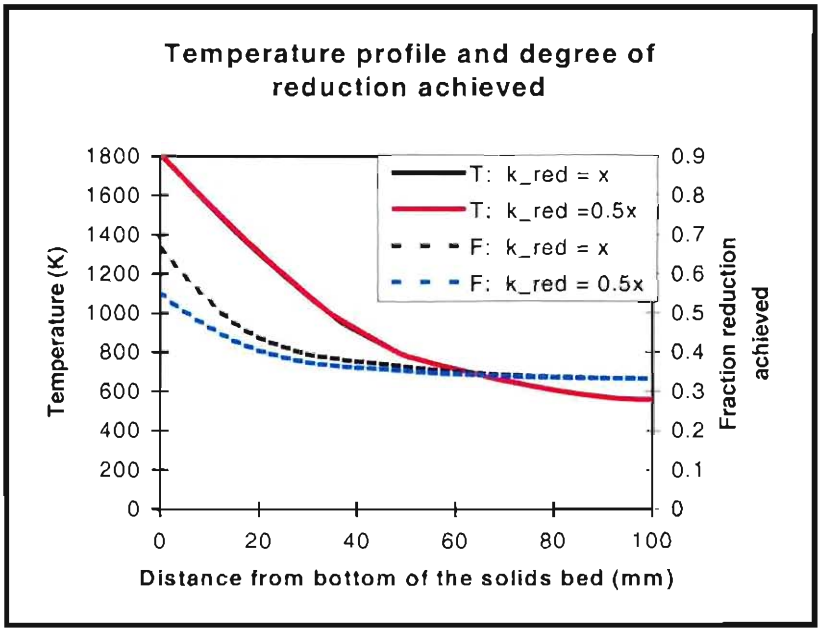

***Figure E 2**: Theoretical profiles of temperature and fraction reduction achieved through a 100mm high solids bed, for a production rate of 30kg/m^2/h, when halving the rate constant for the reduction reaction.*

E.2 Change in rate constant for the gasification reaction

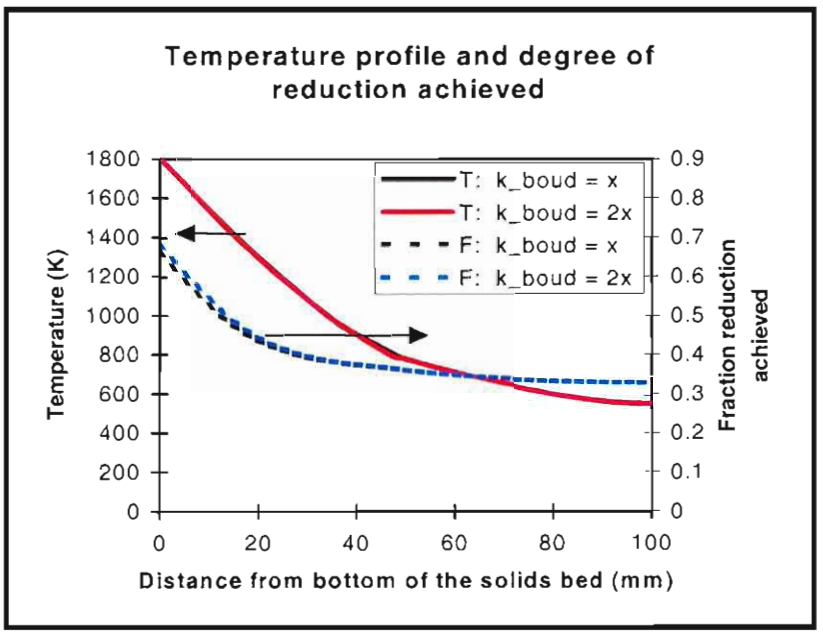

Figure E 3: *Theoretical profiles of temperature and fraction reduction achieved through a 100mm high solids bed, for a production rate of 30kg/m²/h, when doubling the rate constant for the gasification reaction.*

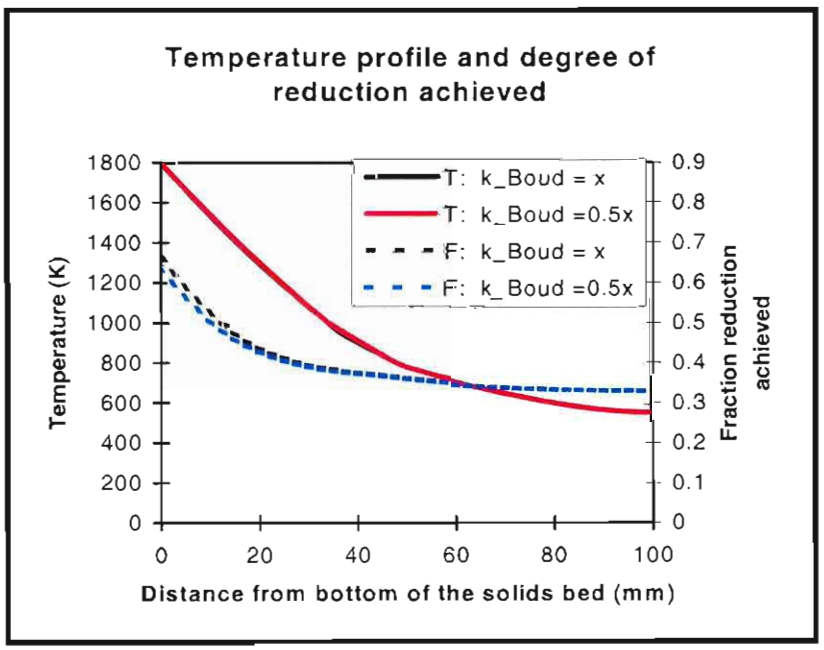

Figure E 4: *Theoretical profiles of temperature and fraction reduction achieved through a 100mm high solids bed, for a production rate of 30kg/m²/h, when halving the rate constant for the gasification reaction.*

E.3 Change in thermal conductivity of the bed

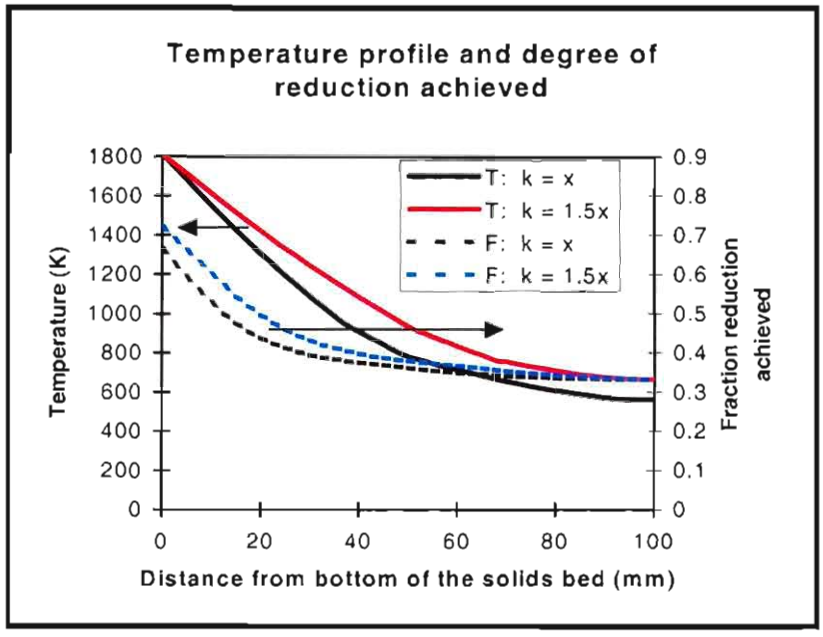

Figure E 5: *Theoretical profiles of temperature and fraction reduction achieved through a 100mm high solids bed, for a production rate of 30kg/m²/h, when increasing the thermal conductivity of the solids bed 1.5 times.*

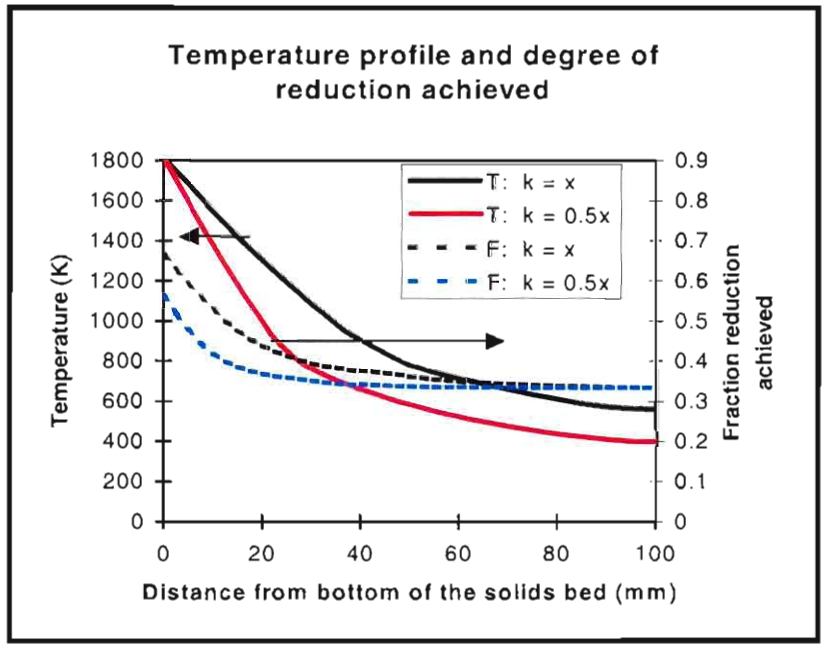

Figure E 6: *Theoretical profiles of temperature and fraction reduction achieved through a 100mm high solids bed, for a production rate of 30kg/m²/h, when halving the thermal conductivity of the solids bed.*

E.4 Change in bath temperature

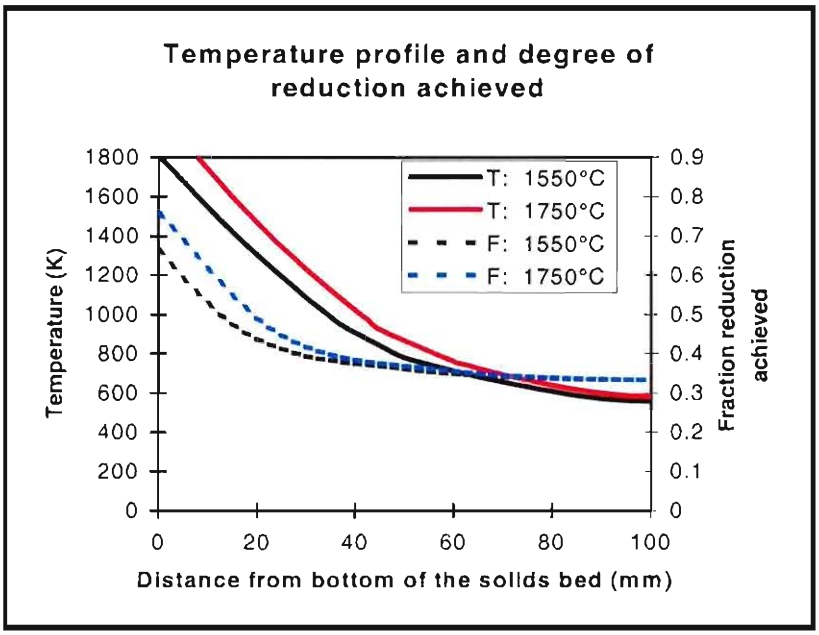

Figure E 7: *Theoretical profiles of temperature and fraction reduction achieved through a 100mm high solids bed, for a production rate of 30kg/m^2/h, when increasing the bath temperature from 1550°C to 1650°C.*

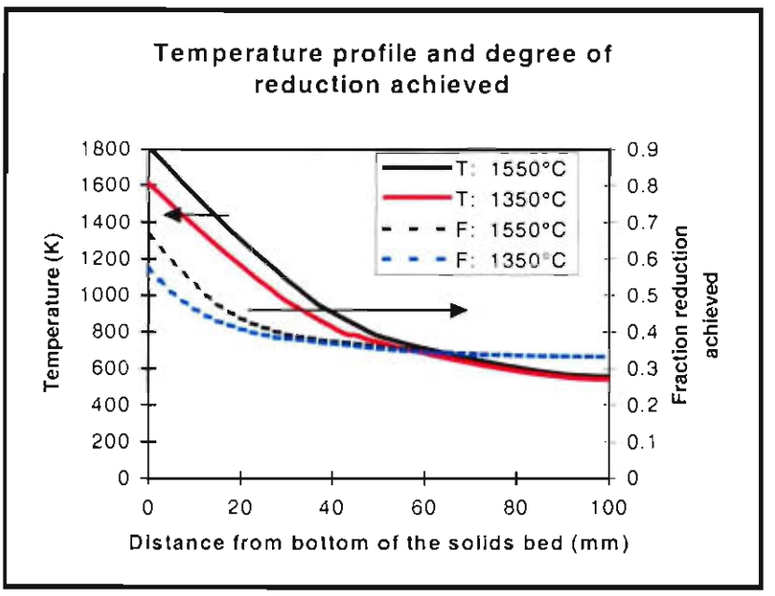

Figure E 8: *Theoretical profiles of temperature and fraction reduction achieved through a 100mm high solids bed, for a production rate of 30kg/m²/h, decreasing the bath temperature from 1550°C to 1350°C.*

E.5 Change in production rate

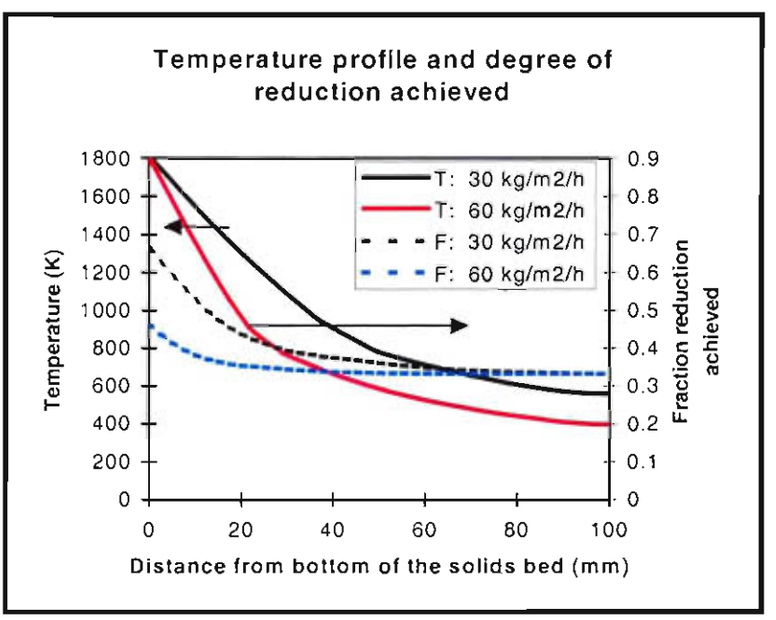

Figure E 9: *Theoretical profiles of temperature and fraction reduction achieved through a 100mm high solids bed, for a production rate of 30kg/m²/h as well as 60kg/m²/h.*

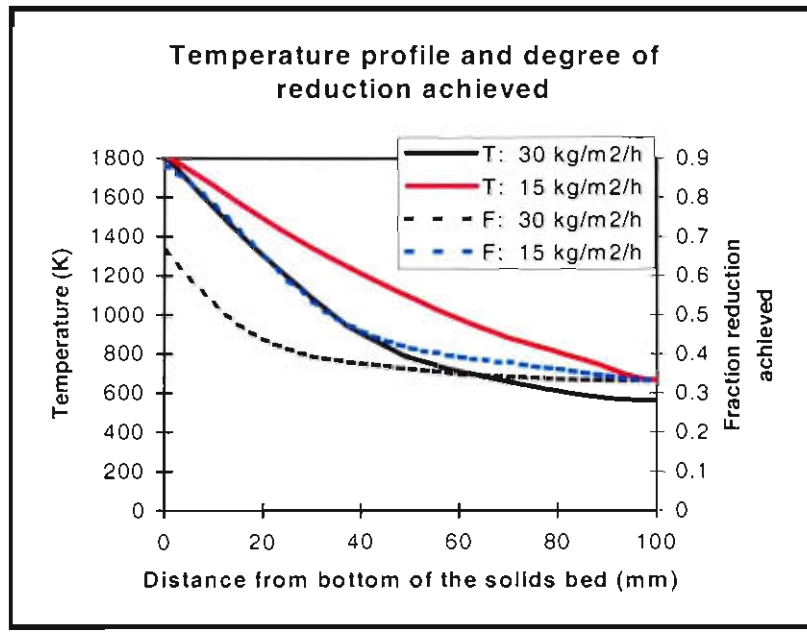

Figure E 10: *Theoretical profiles of temperature and fraction reduction achieved through a 100mm high solids bed, for a production rate of 30kg/m^2/h as well as 15kg/m^2/h.*

APPENDIX F

Experimental aspects: Induction furnace

page no

Appendix F: Experimental aspects: induction furnace

F.1. Raw material mixture selection

Although the $FC/O_{(red)}$ ratio for the feed material at the pilot plant was 1.3, this ratio could not be used for the induction furnace experiments. This is because excess carbon is not oxidised on the outer surface of the solids bed in the induction furnace, as was the case in the pilot plant furnace[10].

To choose the material mixture composition in terms of fixed carbon to reducible oxygen ratio, a thermo gravimetric experiment was done. For this, three samples were compiled, with $FC/O_{(red)}$ ratios of 0.85, 1.0 and 1.15 respectively. The samples comprised of iron ore, char, calcinated dolomite (doloma) and calcinated limestone (lime). Burnt fluxes and char was used because it was assumed that devolatilization and calcinations occurred in the upper part of the solids bed[19]. The samples were reacted in the TGA at 1100°C, since this was the expected average temperature in the lower part of the bed. The experimental equipment and procedures discussed in ***paragraph 2.2*** were used for this test.

The samples were reacted until no further mass loss occurred, after which the samples were removed from the furnace and their respective carbon contents were determined with a Leco CS 400 analyser. From the mass loss (comprising mainly of loss of carbon and oxygen) and the change in carbon content of the sample, the degree of reduction achieved and the amount of excess carbon remaining in the sample was calculated. These results are shown in ***Figure F 1***

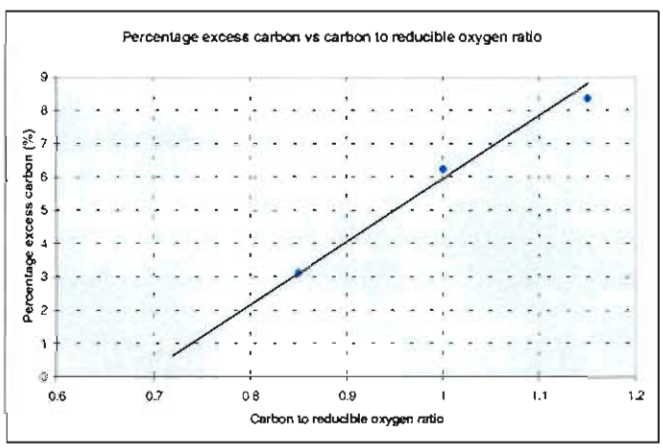

Figure F 1: *Excess carbon in samples as a function of fixed carbon to reducible oxygen ratios*

Figure F 1 shows that a $FC/O_{(red)}$ ratio of 0.7 will yield no excess carbon in the sample. Carbon losses during establishing of the solids bed were estimated at 3% (which was a guess based on pilot plant operations). Accordingly, a fixed carbon to reducible oxygen ratio of 0.85 was chosen for the mixture.

The first seven experiments at the induction furnace (as described in ***paragraph 3.4***) were positioning exercises, during which the experimental equipment and procedure was developed. During these tests the mixture with $FC/O_{(red)}$ ratio of 0.85 was tested to confirm that the mixture would yield a bath with carbon content between 0.01 and 0.1%.

Similar to the way in which the char content of a sample was governed by the $FC/O_{(red)}$ ratio, the doloma and lime content were governed by the anticipated MgO content and basicity of the slag. Since pilot plant trails for the Ifcon process was run with a mixture aiming for 8% MgO in the slag and a CaO/SiO_2 ratio in the slag of 1.4[17], the same criteria was used for this experiment.

The final material mixture selections for simulation of the bottom part of the solids bed in the Ifcon processs are shown in ***Tabel F 1***

Tabel F 1: *Material mixtures used as feed material to the induction furnace*

Feed material	0% pre-reduced mixture	30% pre-reduced mixture	50% pre-reduced mixture
Ore content (%)	78.6	78.2	77.8
Char content (%)	14.3	14.1	14.0
Doloma content (%)	3.4	3.7	3.9
Lime content (%)	3.7	4.0	4.3

F.2. Crucible positioning in the induction furnace

The crucible was positioned so that the surface of the molten bath was at the height of the highest loop of the coil of the inductor. This is the height, above which the induction field deteriorates. Prior to testing, this height was determined by placing six similar mild steel discs in the furnace at various heights, but similar distances from the coil. The

power input to the furnace was set at 20 kW, and the temperature of each metal disc was measured, using a Pt/Pt10%Rh (or type S) thermocouple. From the temperature vs time curves, the heating rate of each disc was calculated. The furnace was cooled and the test was repeated for power inputs of 35 and 50 kW. The results are shown in ***Figure F 2***.

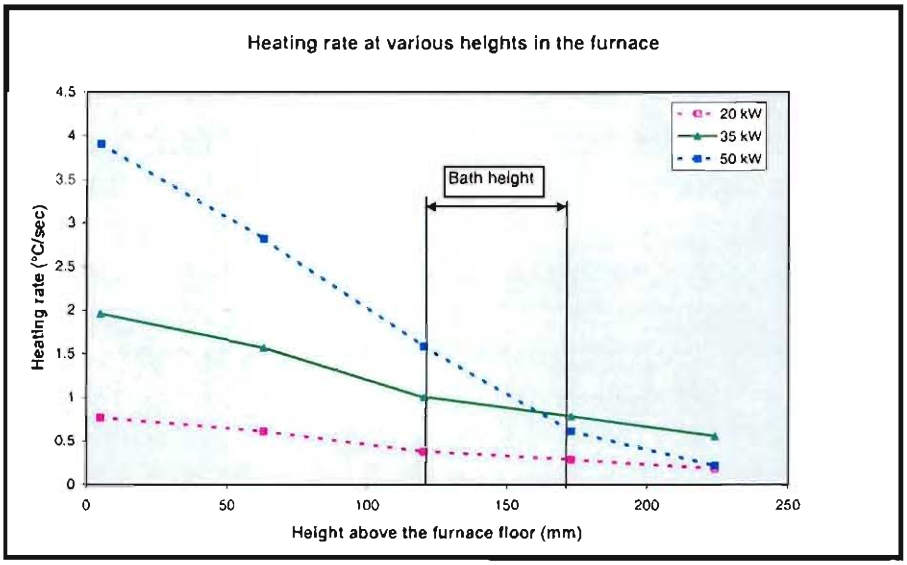

Figure F 2: *Heating rate curve for the induction furnace.*

From the heating rate curves, the height at which the induction field deteriorates (the heating rate curve flattens) was obtained. Since a heat input of about 35kW was anticipated, the bath was established 30 cm below the reference floor height.

During initial test work, attempts were made to establish a metal bath at different heights in the furnace. For this, a trail and error approach was followed. The bath height position determined by this trail and error method was similar to that determined by heating of the discs (as discussed above).

F.3. Calibration of Rotameters with a Bunsen tower.

The method used was similar to the technique discussed in ***Appendix A.1***. However, due to the relatively high flow rates required, a 1000cm^3 Bunsen tower was used. Two rotameters were calibrated, one for the argon purge-gas line and one for the exit-gas line. Since only argon was used as purge gas, the rotameter in the purge-gas line was calibrated with argon. The gas mixture passing through the exit-gas line was expected to be a mixture comprising mainly of argon and carbon monoxide. Accordingly, argon and

carbon monoxide was used to calibrate the rotameter in the exit-gas line. Since the exit gas mainly comprised of argon (± 80%), the calibration curve for argon was used to calculate molar mass flows of species. The calibration curves are shown in ***Figure F 3***.

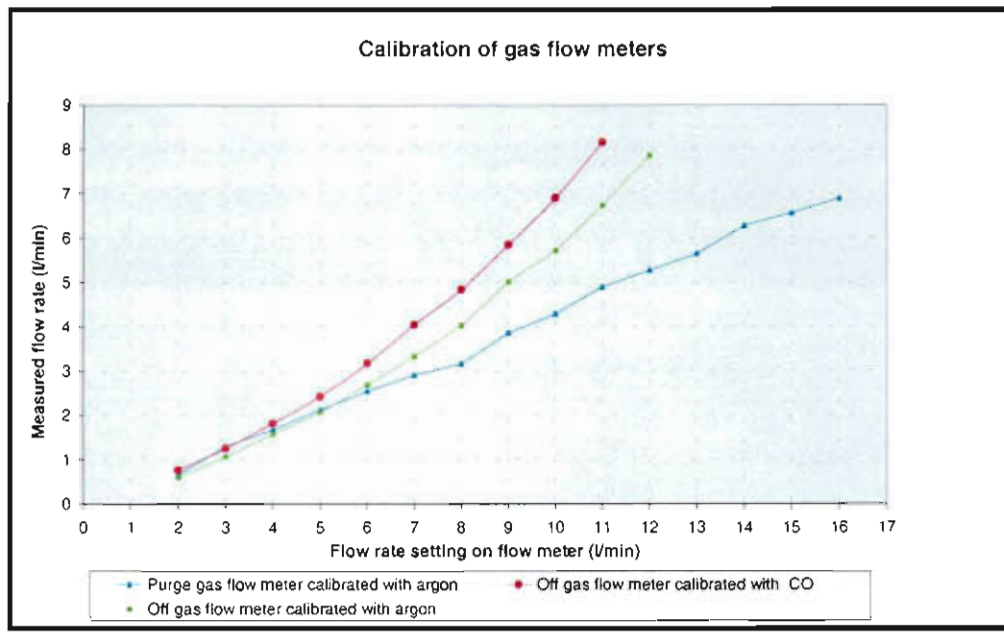

Figure F 3: *Calibration curves for rotameters*

F.4. Visual images from sample cross sections.

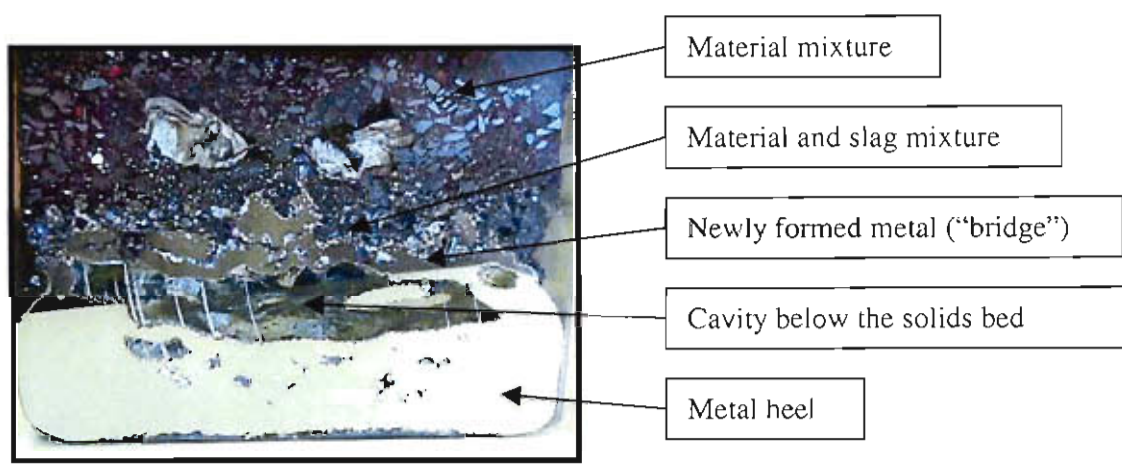

Figure F 4: *Visual image of an impregnated cross section of a sample*

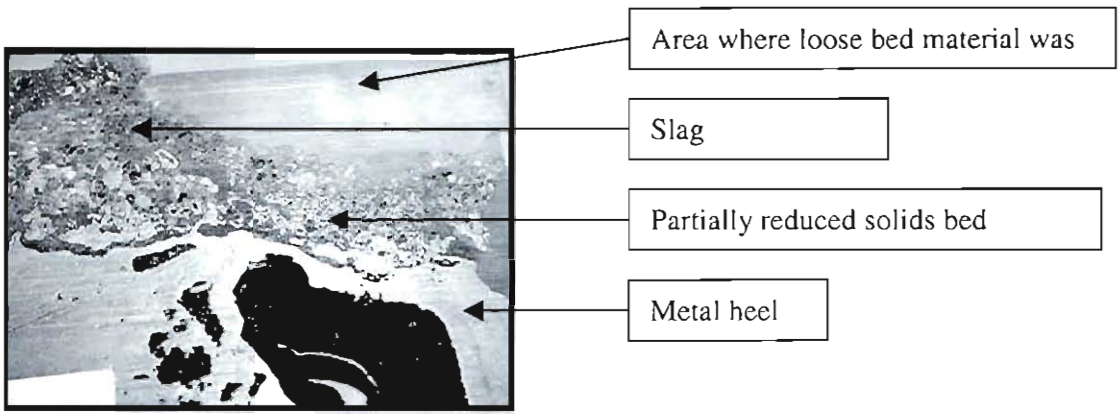

Figure F 5: *Visual image of an impregnated cross section of a sample*

F.5. Gas analyses measured during test work.

The gas analyses obtained are presented in Table F 2 to Table F 5. These analyses were used

Tabel F 2: *Gas analysis from test done with 0% pre-reduced material, during which a production rate of 20 kg Fe /m²/h was achieved.*

Time	Gas composition			
	Ar	CO	CO_2	N_2
	(%)	(%)	(%)	(%)
12:09:46	5.94	5.55	3.69	54.37
12:17:38	42.21	23.97	27.15	4.94
12:23:49	54.15	19.40	20.86	4.19
12:30:00	57.16	14.66	23.70	3.47
12:36:10	61.29	16.52	19.27	1.91
12:42:19	57.04	21.91	18.71	1.60
12:48:32	61.66	19.49	15.37	2.27
12:54:45	62.02	19.11	16.51	1.60
13:00:57	64.98	18.61	14.04	1.71
13:07:09	69.03	12.18	16.05	1.91
13:13:22	68.65	13.81	15.13	1.78
13:19:36	50.44	32.20	15.61	0.87
13:25:48	66.08	17.00	14.34	1.49
13:32:01	70.08	15.26	12.31	1.62
13:38:14	71.81	14.83	10.11	2.51
13:44:27	73.18	15.54	8.52	2.04
13:50:41	73.49	16.69	6.37	2.72
13:56:55	38.69	42.60	15.09	1.44
14:03:07	28.05	45.31	23.75	0.80
14:09:18	54.07	34.67	8.47	1.50
14:15:30	27.45	11.46	8.72	44.65
14:43:06	18.67	41.13	20.63	15.72
14:49:15	57.31	21.25	16.74	3.12

Tabel F 3: *Gas analysis from test done with 0% pre-reduced material, during which a production rate of 55 kg Fe /m²/h was achieved.*

Time	Gas composition			
	Ar	CO	CO_2	N_2
	(%)	(%)	(%)	(%)
11:40:27	5.48	5.22	3.55	55.78
11:46:41	5.88	5.78	4.20	55.95
11:52:53	5.88	5.80	4.38	56.19
11:59:05	5.56	5.76	4.28	56.21
12:05:15	5.29	5.04	4.10	57.34
12:11:21	4.56	4.19	3.42	61.24
12:17:26	3.81	3.15	2.64	66.03
12:23:31	3.33	2.43	2.16	69.15
12:29:36	3.01	1.95	1.84	71.22
12:35:43	2.81	1.62	1.64	72.51
12:43:23	28.02	41.07	18.40	6.89
12:49:34	40.67	30.90	24.93	1.20
12:55:44	56.38	20.24	20.55	1.41
13:01:54	53.36	24.91	19.29	1.17
13:08:04	3.22	55.36	0.98	18.82
13:14:19	46.06	33.27	18.93	1.06
13:22:15	47.64	35.47	11.45	3.72
13:28:27	57.03	22.02	18.03	1.70
13:34:38	41.58	36.24	20.05	1.05
13:40:48	44.14	36.77	16.70	1.08
13:47:00	53.19	31.41	12.99	1.39
13:53:12	54.06	31.50	11.85	1.62
13:59:24	60.01	21.34	15.42	2.09

Tabel F 4: *Gas analysis from test done with 30% pre-reduced material, during which a production rate of 19 kg Fe /m²/h was achieved.*

Time	Gas composition			
	Ar	CO	CO_2	N_2
	(%)	(%)	(%)	(%)
13:52:37	27.05	49.71	15.53	5.95
13:58:51	49.09	35.40	12.05	1.94
14:05:05	57.81	29.86	9.34	1.81
14:11:19	58.56	27.98	9.69	2.27
14:17:32	56.35	30.63	9.90	1.90
14:23:46	60.09	27.18	7.71	3.33
14:30:00	60.13	25.86	10.81	2.05
14:36:13	61.07	25.49	10.23	2.03
14:44:04	32.72	52.71	12.13	0.85
14:50:18	31.10	56.71	9.83	0.90
14:56:32	60.47	30.04	6.06	1.70
15:02:48	62.97	28.11	5.93	1.69
15:09:06	55.23	37.01	4.65	1.45
15:15:23	70.00	21.54	4.44	2.92
15:21:40	71.32	21.19	3.78	2.21
15:27:55	66.81	23.98	4.71	3.16
15:34:10	64.16	26.41	4.55	3.18
15:40:31	64.30	27.53	4.77	2.03
15:46:45	47.26	42.65	7.12	1.74
15:52:58	73.62	18.33	4.60	2.29
15:59:12	76.64	14.61	3.97	3.62
16:08:45	66.92	23.66	2.67	4.75
16:15:02	66.06	12.90	4.44	14.54

Tabel F 5: *Gas analysis from test done with 50% pre-reduced material, during which a production rate of 18 kg Fe /m²/h was achieved.*

Time	Gas composition			
	Ar	CO	CO_2	N_2
	(%)	(%)	(%)	(%)
12:49:57	47.87	13.32	5.45	25.61
12:59:44	46.41	12.43	5.14	27.69
13:09:30	47.29	11.04	4.16	29.25
13:19:04	49.96	9.67	3.59	29.12
13:28:38	48.74	8.31	3.49	30.95
13:38:15	49.51	7.83	3.20	31.29
13:47:51	51.01	6.92	2.71	31.30
13:57:28	51.95	6.19	2.43	31.36
14:07:05	51.71	5.96	2.36	31.87
14:16:41	51.42	2.09	1.06	36.99
14:28:43	46.43	6.90	3.18	34.72
14:38:21	45.23	7.45	3.23	35.25
14:47:58	43.10	8.62	3.44	35.83
14:57:41	43.97	6.69	3.02	36.83
15:07:19	40.79	9.01	3.73	37.08
15:16:54	11.91	30.08	5.17	41.67
15:26:30	28.14	14.21	3.35	43.22
15:36:12	34.14	8.17	3.06	43.52
15:45:50	36.28	7.03	2.70	43.24
15:55:28	37.49	6.51	2.36	42.91
16:05:11	39.62	5.26	1.86	42.69
16:14:49	41.59	4.27	1.46	42.15
16:24:33	36.01	8.51	2.65	42.27

F.6. Temperature profiles through the solids bed.

The Temperatures measured in the solids bed of various experiments are presented below.

Tabel F 6: *Temperature profile of 0% pre-reduced material with which a production rate of 20 kg Fe /m²/h was achieved.*

Trail 1	
Height above metal bath	**Temperature**
(mm)	**(°C)**
84	653
79	
74	660
69	
64	667
59	
54	677
49	
44	757
39	795
34	873
29	
24	980
19	1068
14	1155
9	1228
4	1324

Tabel F.7: *Temperature profile of 0% pre-reduced material with which a production rate of 55 kg Fe /m²/h was achieved.*

Trail 1	
Height above metal bath	**Temperature**
(mm)	**(°C)**
21	814
16	913
11	1074
6	1193
1	1323

Tabel F 8: *Temperature profile of 30% pre-reduced material with which a production rate of 19 kg Fe /m²/h was achieved.*

Trail 1	
Height above metal bath	**Temperature**
(mm)	**(°C)**
47	744
42	
37	856
32	
27	1027
22	1145
17	1260
12	1329
7	
2	

Tabel F 9: *Temperature profile of 50% pre-reduced material with which a production rate of 18 kg Fe /m²/h was achieved.*

Trail 1		Trail 2		Trail 3	
Height above metal bath	Temperature	Height above metal bath	Temperature	Height above metal bath	Temperature
(mm)	(°C)	(mm)	(°C)	(mm)	(°C)
61	755	75	625	68	650
51	880	70	650	63	770
41	1025	60	740	53	860
31	1110	50	855	43	990
26	1200	40	1000	28	1180
21	1250	35	1065	23	1230
16	1315	30	1170	18	1300
11	1350	25	-273	13	1335
6	1390	20	1300	8	1375
1	1410	15	1340	3	1370
		10	1370		
		5	1405		
		0	1440		